Reconfiguration of Amplitude Driven Dominant Coupling Modes (DoCM) mediated by α-band in Adolescents with Schizophrenia Spectrum Disorders

Stavros I. Dimitriadis[1-6*]

1 Cardiff University Brain Research Imaging Centre (CUBRIC), School of Psychology, College of Biomedical and Life Sciences, Cardiff University, Cardiff, United Kingdom

2 Neuroinformatics Group, Cardiff University Brain Research Imaging Centre (CUBRIC), School of Psychology, College of Biomedical and Life Sciences, Cardiff University, Cardiff, United Kingdom

3 Division of Psychological Medicine and Clinical Neurosciences, School of Medicine, College of Biomedical and Life Sciences,Cardiff University, Cardiff, United Kingdom

4 School of Psychology, College of Biomedical and Life Sciences,Cardiff University, Cardiff, United Kingdom

5 Neuroscience and Mental Health Research Institute, School of Medicine, College of Biomedical and Life Sciences,Cardiff University, Cardiff, United Kingdom

6 MRC Centre for Neuropsychiatric Genetics and Genomics, School of Medicine, College of Biomedical and Life Sciences, Cardiff University, Cardiff, United Kingdom

***Corresponding author**

Dr. Stavros I.Dimitriadis

Cardiff University Brain Research Imaging Centre, School of Psychology, Cardiff University, Cardiff, United Kingdom

Head of Neuroinformatics Group

Email: stidimitriadis@gmail.com / DimitriadisS@cardiff.ac.uk

Abstract:

Electroencephalography (EEG) based biomarkers have been shown to correlate with the presence of psychotic disorders. Increased delta and decreased alpha power in psychosis indicate an abnormal arousal state. We investigated brain activity across the basic EEG frequencies and also dynamic functional connectivity of both intra and cross-frequency coupling that could reveal a neurophysiological biomarker linked to an aberrant modulating role of alpha frequency in adolescents with schizophrenia spectrum disorders (SSDs).

A dynamic functional connectivity graph (DFCG) has been estimated using the imaginary part of phase lag value (iPLV) and correlation of the envelope (corrEnv). We analyzed DFCG profiles of electroencephalographic resting state (eyes closed) recordings of healthy controls (HC) (n=39) and SSDs subjects (n=45) in basic frequency bands $\{\delta,\theta,\alpha_1,\alpha_2,\beta_1,\beta_2,\gamma\}$. In our analysis, we incorporated both intra and cross-frequency coupling modes. Adopting our recent Dominant Coupling Mode (DoCM) model leads to the construction of an integrated DFCG (iDFCG) that encapsulates the functional strength and the DoCM of every pair of brain areas.

We revealed significantly higher ratios of delta/alpha$_{1,2}$ power spectrum in SSDs subjects versus HC. The probability distribution (PD) of amplitude driven DoCM mediated by alpha frequency differentiated SSDs from HC with absolute accuracy (100%). The network Flexibility Index (FI) was significantly lower for subjects with SSDs compared to the HC group.

Our analysis supports the central role of alpha frequency alterations in the neurophysiological mechanisms of SSDs. Currents findings open up new diagnostic pathways to clinical detection of SSDs and support the design of rational neurofeedback training.

Keywords: EEG; multiplexity; chronnectomics; schizophrenia spectrum disorders; cross-frequency coupling

Highlights:

- Ratios of delta/alpha$_{1,2}$ relative power spectrum were significantly higher in SSDs subjects compared to HC
- Probability distribution (PD) of amplitude driven DoCM mediated by alpha frequency differentiated SSDs from HC with 100%
- Network Flexibility index (FI) was significantly lower for subjects with SSDs compared to HC group.

Abbreviations

psychotic-like experiences PLEs

Schizophrenia Spectrum Disorders SSDs

dynamic functional connectivity graph DFCG

imaginary part of phase lag value iPLV

correlation of the envelope corrEnv

integrated dynamic functional connectivity graph iDFCG

dominant coupling mode model DoCM

probability distribution PD

Flexibility Index FI

relative power spectrum RSP

cross-frequency coupling CFC

1. Introduction

Psychosis is characterized by hallucinations and delusions or other positive symptoms which have been seen as the prevalent clinical markers of psychotic disorders like schizophrenia. However, psychotic symptomatology can be seen in both general and clinical populations. Recent research has considered psychosis as a continuum process rather than a categorical 'on/off' clinical state. This dimensional clinical status of psychosis includes psychotic-like experiences, schizotypal symptoms, risk at mental states etc (Van Os et al., 2000; Yung et al., 2003). A recent meta-analytic plan suggests that the predominance of psychotic symptoms in the general population lies at 7% (Linscott and van Os, 2013). These experiences are transitory in 80% of cases, in 20% they are persistent and in 7% they predate the onset of a psychotic disorder (Kaymaz et al., 2012; Linscott and van Os, 2013; Zammit et al., 2013).

Psychotic symptoms within the schizophrenia spectrum comprise of childhood-onset schizophrenia with an age of onset ≤ 12 years like schizoaffective, schizotypal, and schizophreniform disorder. It is more than evident that psychotic symptoms are differentiated between children and adolescents in terms of repetition, intensity and these include anxiety, obsessions etc (Courvoisie et al., 2001). Schizophrenia Spectrum Disorders (SSDs) and subclinical symptoms on the psychosis continuum share cognitive demographic characteristics, cognitive levels and etiological risk factors (van Os et al., 2009; Linscott and van Os, 2013). The aforementioned findings supported that psychosis is a phenotype with persistence symptomatology and an increased severity correlated with clinical symptomatology (van Os and Linscott, 2012). From the current literature, there are no consistent findings to characterize the phenotype of sub-clinical psychosis (Kapil and Barrantes-Vidal, 2015; Rössler et al., 2015). The majority of clinical research over sub-clinical psychosis focused mainly on SSDs probably because of their consistency in the clinical symptomatology of psychosis onset (Tandon et al., 2012). Various types of experiences have not been differentiated on SSDs (Yung et al., 2009). Further, psychotic-like experiences (PLEs) which include hallucinations and delusions are quantitatively similar to clinical psychotic symptoms (DeRosse and Karlsgodt, 2015). However, only a few studies attempted to explore whether psychotic symptoms like auditory hallucinations of non-clinical populations are or not phenotypically similar to clinical populations (Hill et al., 2012).

Cortical dis-/dysconnectivity theory of schizophrenia (Friston et al., 2016) has also been explored with electrophysiological methods. The analysis of multichannel electro (EEG) and magneto-encephalography (MEG) signals provides unique information for a functional

interaction between neural oscillations characterizing brain activity of specific areas within the same frequency (intra-frequency coupling) and between frequencies (cross-frequency coupling; Dimitriadis et al., 2017b,2018c) at high temporal resolution (Canolty and Knight, 2010; von Stein and Sarnthein, 2000; Lisman and Buzsaki, 2008; Dimitriadis et al., 2017b, 2018c). These functional interactions are altered in schizophrenia (Allen et al., 2011). The analysis of EEG at rest demonstrated an increased connectivity pattern in δ (1 – 4 Hz), θ (4 – 8 Hz) and β (13 – 30 Hz) frequencies complementary to a decreased pattern in α frequency within the frontal cortex ("*hypo-frontality*") in schizophrenic patients relative to controls (Ragland et al., 2007 ; Mitchell et al., 2015 ; Mubarik and Tohid, 2016). An additional potential biomarker for schizophrenia is *abnormal brain asymmetry* (Oertel-Knoechel et al., 2012; Gotts et al., 2013; Ribolsi et al., 2014; Miyata et al., 2012).

A recent EEG study at resting-state explored aberrant static functional brain connectivity induced by schizophrenia adopting three connectivity estimators, alternative network metrics, and two reference systems (Olejarczyk and Jernajczyk, 2017). The whole connectivity analysis focused on five frequencies: 2–4 Hz (δ), 4.5–7.5 Hz (θ), 8–12.5 Hz (α), 13–30 Hz (β), 30–45 Hz (γ). The authors revealed the inter-hemispheric asymmetric group-difference using Directed Transfer Function granger causality estimator at resting-state. Another study proposed a methodology of selecting the best set of EEG sensors based on their connectivity profile with the rest of EEG sensors to design an optimal classifier for the discrimination of healthy controls (twenty - five) from schizophrenic patients (twenty - five) (Dvey-Aharon et al., 2017). These authors conducted connectivity analysis based on the correlation between pair-wise time series in a broadband frequency of 0.1 Hz-30 Hz. They reported a classification performance of 93.8%. The main disadvantage of both studies was the use of a static connectivity analysis approach versus a more dynamic one that has the advantage of harnessing the high temporal resolution of the EEG modality. Moreover, only the first study explored static connectivity analysis within specific frequencies while both did not explore any cross-frequency interactions, missing important parts of the rich information contained in the human EEG/ MEG (Dimitriadis et al., 2015a, 2016a,b, 2018a,c,d).

A recent study revealed distinct electroencephalographic patterns of delta/alpha brain activity in psychotic disorders including schizophrenia, bipolar disorder, and methamphetamine-induced psychotic disorder (Howells et al., 2018). Delta synchronization is expressed with an increment of EEG delta activity, which has been reported in ScZ and bipolar disorder (Howells et al., 2018). Patients with schizophrenia have shown reduced delta wave activity also in sleep stages 3 and 4 (Sekimoto et al., 2010) and also during the perception of

neutral and emotionally salient words (Alfimova and Uvarova , 2008). Previous studies showed higher delta synchrony during resting eyes closed condition for ScZ when compared with controls (Borisov et al., 2005). Few studies in ScZ have reported relative delta synchronization during rest with open eyes or during the completion of a cognitive task (Basar et al., 2013a,b). We expect to see also delta synchronization (increased relative power) in SSDs subjects that will be studied here (hypothesis I).

Alpha desynchronization is expressed via a decrement of alpha activity, has been reported in ScZ and bipolar disorder (Howells et al., 2018). In ScZ, alpha desynchronization is reported in un-medicated, medicated ScZ adolescent - onset ScZ and first-episode ScZ and (John et al., 2002). Alpha synchronization is a marker of healthy resting wakefulness which reflects the readiness of the brain to process salient information (Klimesch et al., 1999). The exaggerated desynchronization of alpha activity at resting-state in psychotic disorders represents probably an inappropriate readiness to attend and process salient or not information, whether internal or external (Klimesch et al., 1999). We expect to see also alpha desynchronization (decreased relative power) in SSDs subjects that will be explored here (hypothesis II). Motivated by a recent study (Howells et al., 2018), we will estimate also the ratio of Relative Signal Power (RSP) between δ frequency and the two α subbands.

A consistent decreased functional connectivity pattern in the α-frequency band has been reported in ScZ (Di Lorenzo, et al., 2015 ; Tauscher et al.,1998). Interestingly, two studies reported a high correlation between functional connectivity at rest in the α-frequency band with symptoms of ScZ (Hinkley et al., 2011 ; Merrin and Floyd, 1996). Preliminary evidence suggests that β-band functional connectivity is influenced by illness progression and clinical symptomatology (Di Lorenzo, et al., 2015). However, no study that analysed also cross-frequency coupling in conjunction with within frequencies coupling using EEG in SSD.

We hypothesized that the construction of an integrated Dynamic Functional Connectivity Graph (iDFCG) with the incorporation of dominant intrinsic coupling modes (DoCM) which can be either intra or inter-frequency coupling estimations (cross-frequency couplings) will reveal significant features related to SSDs (Dimitriadis et al., 2017b, 2018c). iDFCG tabulates both the strength and the type of interaction between every pair of sensors at every temporal segment. Our analysis will focus on phase-to-phase/amplitude-to-amplitude within frequency couplings and phase-to-amplitude/amplitude-to-amplitude cross-frequency couplings. We expected that the probability distribution (PD) of DoCM related to cross-frequency interactions will be higher for SSDs patients than their healthy controls counterparts mostly in lower frequencies (Sharp and Hendren, 2007) (hypothesis III). The ratio of cross-frequency

interactions versus the total number of existing functional interactions can be seen as a nonlinearity index of dynamic functional information flow indicator of resting-state. We also assumed that SSDs patients will demonstrate a less flexible global brain pattern based on the fluctuation of DoCM across experimental time compared to healthy controls (hypothesis IV). Our final hypothesis is that amplitude and phase-based DoCM will dissociate their distinct role in both groups (hypothesis V). Our hypothesis is supported by recent evidence about the sensitivity of phase-based intrinsic coupling modes in disorders with functional alterations while amplitude-based intrinsic coupling modes showed predominant sensitivity to structural alteration (Engel et al., 2013). Here, we attempted to detect consistent patterns of brain activity and connectivity in adolescents with SSDs with a non-invasive method, EEG, following for the very first time a multiplex scenario via our DoCM model. Our analysis will dissociate the role of amplitude-based and phase-based connectivity patterns under this framework in SSDs.

2. Material and Methods

2.1 Sample Characteristics

The sample for this study is obtained from a public database (http://protein.bio.msu.ru/~akula/korsak/Korsak-eng.htm.). Clinical evaluation of these adolescents with disorders was provided by experts from the National Center of Mental Health of the Russian Academy of Medical Sciences. They were diagnosed according to ICD–10 in Mental Health Research Center, Moscow and it originally consisted of 125 boys 8–15 years old. The diagnosis was schizophrenia, childish type (F20), schizotypal disorder (F21), and schizoaffective disorder (F25).

The sample is divided into a healthy group and a group with symptoms of schizophrenia. The subjects were adolescents who had been screened by psychiatrists and divided into a healthy group (n = 39) and a group with symptoms of schizophrenia (n = 45). Both groups included only two groups of Russian (Moscow) school children boys aged 10-14 year. The age of the group with schizophrenia spectrum disorders (SSDs) (schizophrenia (childhood-onset), schizotypic disorder, or schizoaffective psychosis) with comparatively homogeneous symptoms ranged from 10 years and 8 months to 14 years (12.3 ±1.2 years).

The healthy control group included 39 healthy schoolboys aged from 11 years to 13 years and 9 months. The mean age of the healthy control group was (12.3±1.3 years). SSD group is recorded even before the pharmacological treatment appointments while subjects have been selected with the same severity. The two groups didn't differ in their age.

2.2 EEG Recordings

EEG activity was recorded from 16 EEG channels at resting-state with eyes closed. The electrode positions are demonstrated in Figure 1. The 16 EEG electrodes were placed according to the international 10–20 system rules at the following locations: O1, O2, P3, P4, Pz, T5, T6, C3, C4, Cz, T3, T4, F3,F4, F7, and F8 and monopolar referenced to coupled ear electrodes.

The sampling rate is 128 Hz and the recording time was 1 min giving a total of [60 secs x 128] = 7,680 samples. EEG recordings can be downloaded from the website: http://brain.bio.msu.ru/eeg_schizophrenia.htm. EEG time series were re-referenced to the average reference electrode (Nunez and Srinivasan, 2006) before preprocessing steps.

Parents of the participants have given their informed consent for the participation of adolescents in the original study.

The program of experiments has been approved by the local ethical committee of the Moscow Mental Health Scientific Center of the Russian Academy of Medical Sciences.

For further details see the following article (Kulaichev and Gorbachevskaya, 2013).

2.3 Artifact Reduction with Independent Component Analysis (ICA) and Wavelets

EEG resting-state activity was corrected for artifacts via well-described procedure. We used the entire 1 min recordings of 7680 time points to the artifact correction pipeline. First, we removed line noise using a notch filter at 50 Hz and (Delorme and Makeig, 2004). We adapted independent component analysis (ICA) and the extended Infomax algorithm implemented in EEGLAB (Delorme and Makeig, 2004). The outcome of this procedure is 16 independent components with a characteristic topography and time course. A given independent component (IC) time course from each IC was further decomposed with discrete wavelet transform and Daubechies wavelet filters. Wavelets decomposed every broadband activity of the IC time series into subcomponents with characteristic carrier brain frequency. Wavelet decomposition of IC time course has been realized in 60 temporal segments of 1 sec each to capture in more detail the contamination of an artifact. Artifacts could be detected on specific scalp locations contaminating one frequency or in broaden brain locations and contaminating more than one frequency. Every wavelet subcomponent of an IC is classified as real brain activity or artifactual activity that could be: ocular, muscle, or cardiac artefacts.

We estimated kurtosis and skewness values in temporal non-overlapping windows of 1 sec for every wavelet subcomponent of an IC. The set of 60 values (60 temporal segments of 1 sec = 128 time points) for both metrics was further z-scored and temporal segments of 1s with zscoring values ±2 were classified as artifactual temporal segments (Dimitriadis et al., 2015).

Then, we zeroed those particular temporal segments for specific wavelet subcomponents of an IC. Then, cleaned IC time courses were recomposed from their cleaned wavelet subcomponents. Finally, cleaned wavelet-ICA EEG activity was composed of the cleaned IC time courses.

Apart from this automatic pipeline, we visually inspected IC and wavelet-based time-courses and the related scalp topography of every IC to further validate the correction. Power spectrum analysis of every EEG time course before and after the correction revealed more pronounced characteristic peaks. The correlation of the original time course with its corrected wavelet+ICA version in the time domain was above 0.75 on average compared to the ICA only corrected time series which was below 0.3 on average. So, wavelet-ICA maintains better the temporal structure of the broadband activity.

We additionally validated the proposed scheme by estimating the signal-to-noise ratio (SNR). SNR was estimated by dividing the power spectrum in the frequency domain within every frequency range from the denoised time series with the power spectrum of the original noisy time series. The following equation defines the SNR:

$$SNR = \frac{S}{N} \quad (1)$$

Where S is the power spectrum of the desired cleaned EEG time series and N the power spectrum of the noisy original time series. Before estimating N, we subtracted the power related to the noisy temporal segments detected with our wavelet+ICA method.

We adopted a wavelet-ICA approach for denoising EEG signals with the advantage of not zeroing a whole ICs but only specific temporal segments of 1 sec on wavelet decomposed subcomponents related to specific brain frequencies and extracted via a wavelet transform over each ICs. Figure 1 illustrates the topology of the EEG sensors.

[Figure 1 around here]

2.4 Signal Power Analysis

We estimated the relative power spectrum (RSP) of every EEG sensor and frequency band in both groups. Welch's algorithm was adopted using MATLAB function pwelch leading to the estimation of power spectrum per frequency band first and then their percentage across the total power spectrum leading to RSP. Group statistical analysis across sensors and frequency bands has been performed with Wilcoxon Rank Sum test ($p < 0.05$, Bonferroni corrected, p'<

p/(16*7) where 16 refers to EEG sensors and 7 is the number of the studying frequency bands).

Motivated by a recent study (Howells et al., 2018), we estimated also the ratio of RSP between δ frequency and the two α subbands. Group statistical analysis was performed with the Wilcoxon Rank Sum Test ($p < 0.05$, Bonferroni corrected, $p' < p/(16*2)$ where 16 refers to EEG sensors and 2 is the number of ratios). Characteristic individual alpha peaks were also estimated from the sensor's spectrum profile of every EEG sensor (Corcoran et al., 2018; see supp.material).

2.5 Dynamic imaginary part of phase locking value (iPLV)/ correlation of the envelope (corrEnv) estimates: the Integrated Dynamic Functional Connectivity Graph (IDFCG) based on iPLV and corrEnv (DIFCG^{iPLV}/ DIFCG^{corrEnv} graph)

Here, we describe our dominant intrinsic coupling model (DoCM) presented in the majority of functional neuroimaging modalities (Antonakakis et al., 2017a; Dimitriadis, 2017b, 2018c,2018d). The goal of the DoCM model is to extract the dominant coupling mode between every pair of EEG sensors here and across temporal segments. DoCM model defines the dominant coupling mode across intra-frequency phase-to-phase coupling and inter-frequency phase-to-amplitude coupling modes.

We studied dynamic functional connectivity across experimental time and the 16 EEG sensors within and between the seven studying frequency bands $\{\delta, \theta, \alpha_1, \alpha_2, \beta_1, \beta_2, \gamma\}$ defined, respectively, within the ranges {0.5–4 Hz; 4–8 Hz; 8–10 Hz; 10–13 Hz; 13–20 Hz; 20–30 Hz; 30–48 Hz}. EEG recordings were bandpass filtered with a 3rd order zero-phase Butterworth filter using filtfilt.m MATLAB function.

The width of the temporal window was set equal to 250ms (or 32 samples) and moved forward across experimental time every 46 ms (6 samples) which is adequate to capture both fast and slow oscillations (Dimitriadis et al., 2013a,b,2015a,b,2016a,b,c,2017a,b,2018b,c). Within frequency and between-frequency (cross-frequency) interactions between every possible pair of frequencies were estimated for every temporal segment leading to a quasi-static Functional Connectivity Graph (FCG). This approach leads to 1275 temporal segments and to a dynamic functional connectivity graph (DFCG).

Here, we adopted two connectivity estimators to quantify within frequency and cross-frequency interactions: the imaginary part of phase-locking value (iPLV) and the correlation of the envelope (corrEnv).

To exemplify the notion of cross-frequency coupling estimates to the interested readers that are not familiar, we demonstrated an example between δ and α_1 frequencies derived from F3 and F4 EEG sensors from the first healthy control subject. Figure 2 demonstrates the algorithmic pipeline for estimating phase-to-amplitude coupling (PAC) with iPLV estimator. Figure 2 A,D illustrates the time course of the first 5 secs from the F3 and F4 EEG sensor activity, correspondingly. Figure 2B demonstrates the time course of δ activity from the F3 sensor while Figure 2E shows the time source of α_1 activity from the F4 sensor and the δ activity extracted from α_1 activity from the same sensor. δ activity was extracted from α_1 activity using the bandpass filters transfer function coefficients used to get δ activity from the F3 sensor. Figure 2F shows the δ activity within α_1 activity from the F4 sensor while Figure 2G shows its phase temporal course extracted via Hilbert transform. The phase time course of δ activity from the F3 sensor is illustrated in Figure 2C while both targeted phase time series are shown in Figure 2H. The last sub-figure 2I presents the phase difference of the two targeted phase time series from which iPLV will quantify PAC strength. Intra-frequency coupling with iPLV is estimated using the phase difference time series as shown in Figure 2I derived from two time series with the same frequency content. The whole procedure is repeated for 21 cross-frequency coupling estimates for both CFC estimators and in a dynamic fashion. The 7 within frequency couplings have been estimated between the phase temporal course from two times series with the same frequency content using iPLV.

Figure 3 is devoted describing the algorithmic steps of amplitude-to-amplitude coupling (AAC) between pairs of frequencies as a second complementary cross-frequency coupling estimator. Figure 3A,D refers to the same time courses as in Figure2A,D from the first 5 secs from F3 and F4 EEG sensors. Figure 3B illustrates the δ activity from the F3 sensor and its related envelope extracted via the Hilbert transform. Figure 3E illustrates the α_1 activity from the F4 sensor and its related envelope extracted via the Hilbert transform. Figure 3C and F show the envelopes from F3 and F4 sensors, correspondingly while Figure 3G demonstrates both envelopes in a common plot. AAC is estimated between those time courses via a correlation envelope analysis (corrEnv). Intra-frequency coupling with corrEnv is estimated between pairs of envelopes extracted from time series with the same frequency content. The whole procedure is repeated for 21 cross-frequency coupling estimates for both CFC estimators and in a dynamic fashion. The 7 within frequency couplings have been estimated between the envelope temporal course from two time series with the same frequency content using corrEnv.

[**Figure 2,3 around here**]

This procedure which is described in detail in our previous papers and also aforementioned (Dimitriadis and Salis, 2017b;Dimitriadis et al., 2018c), resulted in 7 $DFCG^{iPLV}$/ $DFCG^{corrEnv}$ per participant for within frequency bands and 21 $DFCG^{iPLV}$/ $DFCG^{corrEnv}$ per participant for each possible cross-frequency pair. 7 $DFCG^{iPLV}$/ $DIFCG^{corrEnv}$ tabulate iPLV/corrEnv estimates between every possible pair of sensors. For each subject, two 4D tensors [frequencies bands 28 × temporal segments × sensors x sensors] were constructed for each subject integrating spatiotemporal phase-based and amplitude-based interactions. The final outcome of this analysis is two 4D fully-weighted tensors per subject. However, not all connections exist. For that reason, we adapted a proper surrogate analysis.

The adopted surrogate analysis focuses on detecting 'true' brain interactions between every pair of sensors and at every temporal segment (snapshot of DFCG) and finally to detect the dominant type of interaction. For this purpose, we constructed 1,000 surrogate time-series by cutting first at a single point at a random location around the middle of the original time series (between 25 s and 35 s), creating two temporal segments and then exchanging the two resulting temporal segments (Dimitriadis and Salis, 2017b ; Dimitriadis et al., 2018c). Surrogate time series was created on the 7 bandpass filtering time series in the amplitude domain and were employed for both connectivity estimators per subject.

$DFCG_{Surr}^{iPLV}$ / $DFCG_{Surr}^{corrEnv}$ were estimated over the 1,000 surrogate time series for both within frequencies and between frequencies interactions, for each pair of sensors and for each temporal segment. $DFCG_{Surr}^{iPLV}$ / $DFCG_{Surr}^{corrEnv}$ are 5D tensors where the 1st dimension refers to 1,000 surrogate values while the rest 2nd -5th dimensions are similar to the 4D tensors of the original $DFCG^{iPLV}$/ $DFCG^{corrEnv}$. Comparing the original value for every EEG sensor pair, for every temporal segment and every coupling mode (28 in total) from the original $DFCG^{iPLV}$/ $DFCG^{corrEnv}$ with the 1,000 surrogates (1st dimension of $DFCG_{Surr}^{iPLV}$ / $DFCG_{Surr}^{corrEnv}$), we assigned a p-value to every potential intrinsic coupling mode. We then correct for multiple comparisons the p-values related to the 28 (21 + 7) possible DoCM in order to reveal a DoCM per pair of EEG sensors and for each temporal segment. There are three scenarios:

1. a no *p*-value survived the multiple corrections ($p' < p/28$)

where $p = 0.05$)

2. we selected the DoCM with the maximum iPLV/corrEnv value if more than one survived,

3. only one coupling mode survived the multiple corrections

Figure 4A demonstrates how DoCMs are defined employing the first two temporal segments from a healthy control subject between F7 and F3 EEG sensors. The surrogate-based analysis revealed α_2-γ phase-to-amplitude coupling (PAC) as the dominant coupling mode (DoCM) among the 28 potential coupling modes for the two very first temporal segments between F3-F7 sensors. Matrices called comodulograms tabulate the strength measured with iPLV for within-frequency couplings (main diagonal) and between-frequencies (off-diagonal). Figure 4B illustrates the fluctuation of DoCM across experimental time for the F3-F7 sensor pair. Y-axis refers to one of the 28 potential coupling modes while the colour refers to the iPLV related strength. The coloured matrix on the right tabulated the probability distributions (PD) of every potential coupling mode across experimental time. $\alpha 1$-α_2 is the CFC with the highest representation across experimental time for this EEG pair of sensors. Flexibility Index (FI) and PD are estimated from semantic time series as the one presented in Figure 4B for every pair of EEG sensors (see next section).

After applying a multiple comparison correction, the strength and also the type of dominant coupling mode are tabulated in 2 3D tensors of size [1275 x 16 x 16] called Integrated Dynamic Functional Connectivity Graph (IDFCG). We used the term integrated to underline the information of DoCM tabulated within these IDFCGs**.** One keeps the strength of the coupling based on iPLV/corrEnv and the second tabulated the dominant coupling mode of interaction using integers from 1 up to 28:1 for δ, 2 for θ, …, 7 for γ, 8 for $\delta - \theta$, …, 28 for $\beta_2 - \gamma\}$ (Figure 4B). We followed the same procedure in the previous studies from our group (Dimitriadis and Salis, 2017b, Dimitriadis et al., 2017c,2018a,b,c,d).

Figure 4B demonstrates the temporal evolution of DoCM (1st 3D tensor) and the related strength (2nd 3D tensor) across experimental time for F7-F3 EEG pair while the comodulogram on the right side tabulates the PD of the DoCM for this semantic time series. FI and PD will be estimated over the 2nd semantic 3D tensor.

In the present study, we adapted the debiased version of PAC as presented in van Driel et al., (2015).

[Figure 4 around here]

2.6 Semantic Features Derived from the evolution of DoCM

This section describes the semantic features that can be extracted by analyzing the 2nd 3D tensor that preserves the DoCM across spatio-temporal dimensions.

2.6.1 Flexibility Index (FI)

We adopted a previously defined estimator called Flexibility index (FI) which quantifies the transition rate of DoCM between every pair of sensors across experimental time (Dimitriadis and Salis,2017b ; Dimitriadis,2018c). FI is estimated based on the 2nd 3D tensor of the DIFCG that tabulates the semantic information of DoCM across the brain and experimental time. This metric will be called hereafter FI^{DoCM} which is defined as:

$$FI^{DoCM} = \frac{no\ of\ transitions}{temporal\ segments - 1} \quad (2)$$

We encountered a transition only between two consecutive temporal segments where a functional coupling exists. The term (temporal segments – 1) refers to the pairs of temporal segments where a functional coupling mode exists. FI counts only the change of the DoCM and not the direction between specific pairs of frequency coupling modes. FI^{DoCM} gets higher values for higher "jumps" of DoCM between a pair of EEG sensors across experimental time. Figure 4B illustrates how FI^{DoCM} is estimated for the F3-F7 EEG pair.
This approach leads to a 16 x 16 matrix per subject or 16^2 =140 FI features. We estimated also the global FI by averaging the 16 nodal FI. FI is estimated from a semantic time series presented in Figure 4B.

2.6.2 Spatiotemporal distribution of DoCM— Comodulograms

Based on the 2nd 3D DIFCG that keeps the semantic information of the preferred dominant coupling mode, we can tabulate in a frequencies × frequencies matrix the probability distribution (PD) of observing each of the DoCM frequencies across 7 (intra-frequency) + 21 (cross-frequency coupling) = 28 possible coupling modes and exploring their spatio-temporal distribution.

The spatiotemporal PD tabulated in a matrix is called hereafter comodulogram and an example is demonstrated in Figure 4B (Antonakakis et al., 2016,2017a,b ; Dimitriadis and

Salis,2017b,c ; Dimitriadis,2018a,c,d). PD is a new vector of features with dimension 1 x 28 possible DoCM. Figure 4B visualizes a PD matrix and demonstrates how it is computed.

2.6.3 Nonlinearity Index (NI) based on DoCM

When two brain areas communicate via within the same frequency (intra) then this interaction is linear. However, cross-frequency interactions are nonlinear pathways of information exchange via brain areas playing a pivotal role important role in inter-areal communication (Tallon-Baudry and Bertrand, 1999; Varela et al., 2001; Breakspear, 2002; Darvas et al., 2006 ; Jensen and Colgin, 2007; Chen et al., 2009,2010). The dissociations between linear coupling (within-frequency coupling) and non-linear coupling (between-frequency coupling) has been also proved via biophysical modeling (Chen et al., 2009,2010).

We first estimated a global PD of dominant coupling modes across space (EEG pairs) and time (temporal segments). This calculation yields a matrix of size 28 (potential coupling modes) x 1275 (temporal segments) per subject. From this global PD matrix, we estimated the sum of PD related to cross-frequency coupling (21 values) versus the sum of PD related to within frequency coupling (7 values). This ratio can serve as a nonlinearity index (NI) of the information flow between brain areas (equation 3). To untangle the role of α modulated frequency as a key driver of any significant group differences, we also estimated the ratio of the sum of PD of cross-frequency couplings between a modulated frequency and the rest of frequencies versus the PD of the within-frequency interactions on the modulated frequency was estimated. Particularly, we estimated the ratio of the sum of PDs between α1 and $\{\alpha_2,\beta_1,\beta_2,\gamma\}$ and between α_2 and $\{\beta_1,\beta_2,\gamma\}$ with the sum of PDs related to α_1 and α_2 within frequencies interactions (equation 4). The NI gets a positive value where the higher it gets the higher is the contribution of CFC to the dominant coupling modes and so the higher the nonlinearity of the communication within the complex system. For group comparisons, we adopted the Wilcoxon Rank-Sum test as a statistical test to compare the distributions of temporal NI.

$$NI^{TOTAL} = \frac{\sum_{n=1}^{\#\ of\ CFC} PD^{CFC}}{\sum_{k=1}^{\#\ of\ within} PD^{within}} \quad (3)$$

$$NI^{\alpha} = \frac{PD^{a1-a2} + PD^{a1-\beta1} + PD^{a1-\beta2} + PD^{a1-\gamma} + PD^{a2-\beta1} + PD^{a2-\beta2} + PD^{a2-\gamma}}{PD^{a1} + PD^{a2}} \quad (4)$$

2.7 Inter-Hemispheric Group Differences of Dynamic Functional Connectivity Strength

We explored how inter-hemispheric dynamic functional strength differed between the two groups. Dynamic functional connectivity strength is a time series of size 1275 that informs us of how functional connectivity strength changes over experimental time. Figure 5A illustrates an example of such a time series for iPLV estimator between F7-F8 EEG sensors from the first healthy control subject. Our analysis focused on functional connectivity strength between the following two sets of EEG sensors, one per hemisphere : Left hemisphere: { O1 P3 T5 C3 T3 F3 F7}, right hemisphere: {O2 P4 T6 C4 T4 F4 F8}. The combination of both sets forms a set of 49 inter-hemispheric links. From every functional connectivity strength time series, we estimated the mean value and also its spectrum using Welch's approach and the related function in MATLAB. For the spectrogram, we extracted the dominant frequency that is a descriptive statistic of the fluctuation of connectivity across experimental time (Figure 5B).

Group statistical analysis was performed with the Wilcoxon Rank Sum Test ($p < 0.05$, Bonferroni corrected, $p' < p/49$ where 49 refers to the total number of inter-hemispheric links).

[Figure 5 around here]

2.8 Group Discrimination via a Machine Learning Approach

We adopted the simplest k-NN classifier to enhance the quality of the features extracted with our DoCM model. PD and FI were integrated into a single feature vector of 284 features (28 : PD + 256 (16x16) : FI).

We classified every subject with k-NN classifier (Knn = 10) following 5-fold cross-validation (CV) scheme running 100 times. As a feature selection algorithm, the infinite feature selection algorithm was selected (Roffo et al., 2015). Feature selection has been applied within every fold of the 5 CV and across runs. From the ranking of 284 features within every fold, we kept the first 10 ranked features. We scored the features that were selected in the first 10^{th} across the 100 runs and 5 folds.

Our analysis was followed independently for iPLV/corrEnv derived PD and FI.

2.9 Software

The analysis has been realized in the MATLAB environment (v2019b) using the signal processing toolbox. Fast ICA has been adopted from the fieldtrip toolbox. Dynamic functional connectivity has been based on in-house software provided on our github website: https://github.com/stdimitr/time_varying_PAC.

3. Results

Our results reported on cleaned EEG brain activity with a combination of ICA and wavelets. SNR values were higher than 6 while no group differences have been estimated at single-channel comparisons (SFigure 1). The high SNR values further support current findings under the framework of connectivity analysis which is affected by SNR.

3.1 Relative Signal Power in HC and SSDs subjects

Statistical comparison of RSP between the two groups across EEG sensor space and frequency bands revealed significantly higher signal power in δ (increased synchronization) and also in θ frequency bands for SSDs compared to HC evaluating our first hypothesis. We found also significant lower RSP values for the SSD group compared to HC in the α_2-frequency band supporting our second hypothesis of reduced alpha desynchronization in SSDs subjects.

Figure 6 illustrates group-averaged RSP in SSDs and HC groups. Comparison of group-averaged Relative Signal Power (RSP) of δ versus RSP of α_1 and α_2 across EEG sensor space in HC and SSDS patients revealed interesting trends. Our analysis revealed a significantly higher ratio RSP of δ / α_1 for SSDS compared to HC in F7 and Cz EEG sensors. Significantly higher ratio RSP of δ / α_2 for SSDS compared to HC was revealed in all the EEG sensors exception for channel T6 (Figure 7) (* Wilcoxon Rank Sum test ($p < 0.01$, Bonferroni corrected, $p' < p/(16*2)$ where 16 refers to EEG sensors and 2 to the number of the ratios). These results supported a distinct role of alpha subbands.

Group-averaged alpha peaks were around 9.03 Hz across EEG sensors. Alpha peaks didn't reveal any group differences trends (SFigure 2).

[Figure 6 and 7 around here]

3.2 Contribution of Semantic Features based on DoCM model for High Classification Performance of SSDs Subjects

Our machine learning strategy revealed 10 consistent features among FI and PD of DoCM in both estimators. Consistent features refer to those features where their Score across 100 runs x 5 – fold CV equal to 500. Figure 8 (a-b) illustrates the spatial distribution of the FI across every possible pair of EEG sensors for the HC and SSDS group while Figure 8 (c-d) illustrates the comodulograms of the PD for the HC and SSDs group tailored to iPLV. Similarly, Figure 9 (a-b) illustrates the spatial distribution of the FI across every possible pair of EEG sensors for HC and SSDs group while Figure 9 (c-d) illustrates the comodulograms of the PD for HC and SSDs group tailored to corrEnv. Interestingly, the most discriminative features were the ones related to PD compared to FI.

Figure 10 illustrates the most discriminative features which are PD for θ-γ, α_1-α_2 θ-β_2 cross-frequency pairs. Every dot refers to a subject presented in a 3D feature space. Based on our findings, we evaluated hypothesis III.

The classification performance based on selected FI+PD features was 74% for iPLV and 100% for corrEnv. The weighed discriminative score of features related to corrEnv was 10 times higher than the features from iPLV which was reflected the absolute accuracy. Moreover, Figure 10 illustrates and evaluates the high classification accuracy between the two groups. Table 1 tabulates the performance of each set of features.

[Figure 8,9 and 10 around here]

[Table 1 around here]

3.3 Global Network Flexibility Index (FI)

By averaging the FI values across both dimensions of the matrix [16 x 16] per subject, we estimated the global network FI as a unique characterization of network flexibility. Group-averaged FI did not reveal significant differences for the iPLV estimator ($FI^{HC} = 0.2104$, $FI^{SSDs} = 0.2085$,pval = 0.0673). However, group-averaged FI revealed significant differences for corrEnv estimator ($FI^{HC} = 0.2466$, $FI^{SSDs} = 0.2123$,pval = 0.00345×10^{-5}). Our results supported our hypothesis IV.

3.4 Nonlinearity Index (NI) of Information Flow based on DoCM

Figure 11 demonstrates the group-averaged Nonlinearity Index for iPLV (Figure 11.A) and corrEnv estimator (Figure 11.B). NI for corrEnv estimator was significantly higher for SSDs compared to HC following a Wilcoxon Rank Sum Test across experimental time ($p = 0.0001274 \times 10^{-12}$). In contrast, the Nonlinearity Index did not differ between the two groups for iPLV ($p = 0.0669$). Statistical analysis has been applied over the temporal mean of NI time series.

[Figure 11 around here]

3.5 Inter-Hemispheric Group Differences of Temporal Functional Connectivity Strength

No group differences have been identified for the dominant frequency of dynamic functional connectivity strength of inter-hemispheric links with both connectivity estimators. However, we found group-averaged differences between the mean values of the following inter-hemispheric links:O1-P4 P3-O2 P3-T6 C3-T6 F3-O2 F3-C4 (Figure 12.A), for iPLV and C3-T6 C3-T4 for corrEnv (Figure 12.B). Group-averaged iPLV values were higher for SSDs while group-averaged corrEnv were higher for healthy controls.

[Figure 12 around here]

4. Discussion

Our DoCM model identified the dominant coupling modes across experimental time and between every possible pair of EEG sensors as a natural way to reveal the multiplexity of brain oscillations. We revealed a delta synchronization (increased signal power) and alpha desynchronization (decreased signal power) in SSDs subjects, which was also evidenced by a higher ratio of relative signal power of delta/alpha$_{1,2}$ for SSDs compared to HC. The PD of DoCM untangled trends between the two groups with more pronounced results in amplitude driven dominant coupling modes. Machine learning results revealed absolute discrimination of SSDs from HC focusing on PD of cross-frequency interactions. This high discriminative power between the two groups is driven by features estimated over amplitude (activity) and alpha frequency driven DoCM (connectivity) which are significlyant higher in SSDs subjects compared to HC. Focusing on DoCM, we defined a novel nonlinearity index of information flow as the ratio of cross-frequency interactions versus the total number of existing

functional interactions, we detected a significantly higher nonlinearity for SSDs compared to HC across the recording time only in the amplitude domain. This result was more pronounced when we focused on alpha frequency. The overall network flexibility was significantly lower in SSD patients compared to HC only in the amplitude domain. Finally, our analysis revealed significant findings for SSDs working with brain activity and the multiplex character of brain connectivity dissociating the distinct role of amplitude and phase coupling modes.

Before disentangling one by one the main findings of this study, it is important to mention here that our denoising algorithm based on the combination of ICA and wavelets increased the SNR of EEG recordings. This result supports our findings based on signal power and also on brain connectivity where connectivity estimators are sensitive to SNR levels (see SFigure 1).

Previous studies showed that patients with schizophrenia have reduced delta wave activity also in sleep stages 3 and 4 (Sekimoto et al., 2010) and also during the perception of neutral and emotionally salient words (Alfimova and Uvarova, 2008). Delta synchronization expressed with an increased EEG delta activity, has been reported in ScZ and bipolar disorders (Howells et al., 2018). Here, we confirmed such a delta synchronization in SSD patients compared to healthy controls (Figure 3). Increased delta activity (delta synchronization) is associated with central nervous system depression, observed during slow-wave sleep, in anesthesia and in com which are all conditions with characteristic decreased levels of consciousness (Englehardt et al., 1991; Hashemi et al., 2015). A global delta increased activity has been linked to the subthreshold activity of GABAergic neurons originating from the thalamic reticular nucleus and lateral geniculate nucleus (Ulrich et al., 2014;Herrera et al., 2016). Increased delta activity has been linked to lesions in basal forebrain during wakefulness (Fuller et al., 2011) combined with cholinergic and serotonergic blockade (Vanderwolf and Pappas, 1980). Pharmacological models for delta activity have reported interesting findings. The use of an acetylcholinesterase inhibitor in Alzheimer's disease decreases delta and theta power while it increases alpha power in the left insula following with a cognitive improvement (Gianotti et al., 2008).

In ScZ alpha desynchronization (decreased alpha activity) is reported in adolescent-onset ScZ, first-episode ScZ and un-medicated, and medicated ScZ (John et al., 2002). We found alpha desynchronization in SSDs subjects compared to healthy controls (Figure 6). It is well-known that desynchronization of alpha activity reflects diverse changes in thalamo-cortical and cortical network communication (Klimesch et al., 1999). Two key subnetworks underlie alpha desynchronization: a) the activation of the visual system, via the reticular activating system

(Volavka et al., 1967) as they were revealed by looking at EEG activity recorded during a subject who opens his eyes (eyes-open resting-state) after an eyes-closed resting-state where there is a mass desynchronization of alpha activity and b) desynchronization of alpha activity reflects different changes in thalamo-cortical and cortico-cortical network communication (Klimesch et al., 1999). Decreased alpha activity (alpha desynchronization) has been also associated with central nervous system depression as a consequence of long term use of alcohol, in anesthesia and vegetative states where all conditions demonstrated decreased levels of consciousness (Hoffman et al., 1995 ; Kaplan et al., 1985 ; Lehembre et al.,2012). In healthy conditions, alpha synchronization is an indicator of healthy resting wakefulness and arousal to attend and also process salient information (Klimesch et al., 1999). Our findings in alpha frequency could be attributed to a loss of alertness and arousal with a possible thalamo-cortical implication. Alpha is generated glutamatergic and muscarinic transmission within the thalamus (Hughes and Crunelli, 2005). Reduced alpha signal power has been seen in cholinergic (Olincy and Freedman, 2012), in glutamatergic (Javitt, 2010) and also in GABAergic (Gonzalez-Burgos and Lewis, 2012) models in schizophrenia.

Studying the ratio of delta/alpha$_{1,2}$, we detected a significantly higher ratio for SSDs compared to HC group similarly to subjects with bipolar disorders and schizophrenia (Figure 7 ; Howells et al., 2018). Our study is the first one that identified these biomarkers in SSDs subjects. Biophysical models on the source space will further evaluate the origin and the explanation of our observations based on delta and alpha relative signal power.

A consistent decreased functional connectivity pattern in the α-frequency band has been reported in ScZ. In particular, decreased α connectivity estimated by coherence, lagged coherence and phase synchrony, has been reported at frontal (Di Lorenzo, et al., 2015 ; Tauscher et al.,1998), fronto-posterior (Di Lorenzo, et al., 2015, Lehmann et al., 2014) and parieto-temporal (Di Lorenzo, et al., 2015) brain areas (for different results see also Andreou et al., 2015;Kam et al., 2013;Winterer et al., 2011;Merrin and Floyd, 1996). Interestingly, two studies reported a high correlation between functional connectivity at rest in the α-frequency band with symptoms of ScZ (Hinkley et al., 2011;Merrin and Floyd, 1996). Contradicting evidence has been reported for fast oscillations in the β- (13– 30 Hz) and γ- (30–200 Hz) frequencies at rest, including both elevated (Di Lorenzo, et al., 2015), reduced (Kam et al., 2013) and intact (Lehmann et al., 2014, Andreou et al., 2015, Tauscher et al., 1998, Winterer et al., 2011) β-band connectivity. Preliminary evidence suggests that β-band functional connectivity is influenced by illness progression and clinical symptomatology (Di Lorenzo, et

al., 2015). For a systematic review tailored to functional connectivity evidence using EEG in schizophrenia see Maran et al. (2016).

Here, we adopted our DoCM model to reveal the dominant coupling modes independently in the amplitude and phase domain. It is well-known the distinct role of amplitude-to-amplitude coupling and phase-to-amplitude coupling between frequencies (Hyafil et al., 2015). Many previous studies explored the contribution of both low and high-frequency oscillations to explain a range of cognitive deficits in schizophrenia modulated with specific frequency content (Moran and Hong,2011). Here, we analyzed phase-to-phase (within frequencies) with phase-to-amplitude couplings (cross-frequencies) in the phase domain and amplitude-to-amplitude couplings of the envelopes of either the same frequency (within frequencies) or of different frequencies (cross-frequencies). Phase based intrinsic coupling modes are band-limited in specific frequency bands, are extended from local to large-scale coupling networks, and changed in disorders with structural or even functional network alterations (Engel et al., 2013). Envelopes of Amplitude based intrinsic coupling modes display a typical frequency range on the ultra-slow spectrum below 0.15 Hz similar to BOLD activity. We typically estimated correlation of the envelope between frequency-dependent brain signals but the spectrum of the envelopes is within that frequency scale. Amplitude based intrinsic coupling modes are extended both locally and globally (network level) and might be severely affected in disorders with a predominant structural network alteration (Engel et al., 2013). Structural brain changes in subtypes in schizophrenia could further support our findings in amplitude driven DoCM which are more sensitive in structural changes (Zhang et al., 2014).

Comparing the findings of PD of DoCM with phase driven (Figure 8) and amplitude driven (Figure 9) frequency-interactions modes, we untangled a reconfiguration of DoCM in the latter case in SSDs subjects driven by alpha sub-bands. Attention can be allocated into a dorsal, top-down network and a ventral, bottom-up network. The top-down network is responsible for attention to certain features while the bottom-up network is mainly stimulus-driven. These networks are identified in both task-based (Corbetta and Shulman, 2002) and resting-state neuroimaging paradigms (Fox et al., 2006) and are directly related to attentional functions that are active even at resting-state conditions. Both types of cross-frequency phase–amplitude coupling (PAC) and amplitude–amplitude coupling (AAC) are highly preserved in top-down and bottom-up networks in macaque auditory cortex (Marton et al., 2019). The most discriminative features of PD of DoCM supported an absolute accuracy of the two groups. Selected features revealed also a complementary role of theta modulating DoCM with higher frequency bands (beta/gamma), an observation that has been reported also in a resting-state

study in HC with MEG modality (Florin and Baillet, 2015). Additionally, we observed a significantly lower global FI in SSDs compared to HC only in amplitude driven DoCM. In a recent lifespan study with healthy controls, we found aberrant FI for two groups, a dyslexic group and a mild traumatic brain injury (Dimitriadis et al., 2019). FI can be seen as a global index of the normal multiplexity behavior of nested oscillations. DoCM, their PD, and other features, where some of them are presented here, are further needed to explain in more detail group differences between healthy controls and targeted groups.

The Nonlinearity Index defined and reported here for the first time showed a higher nonlinearity of resting-state networks for SSDs subjects compared to HC only in the amplitude domain while in phase there was no group difference. Our findings have been consistent both using the whole repertoire of within and between frequencies couplings but also focusing on alpha sub-bands modulators (Figure 11). Our study first dissociates the potential different role of amplitude and phase driven intrinsic coupling modes in general and specifically in the target group of SSDs. These results are supported by findings of a recent study that underlined the complementarity of cortical phase and amplitude coupling patterns. This study revealed also the importance of amplitude coupling measures (Siems and Siegel, 2020). Our results untangled an interesting role of alpha frequency as the key frequency modulator that demonstrates a similar behavioral role in phase coupling modes in both groups and a distinct role in amplitude domain dissociating its role in SSDs from healthy controls. Further research is needed based on biologically inspired models like dynamic causal modeling that will attempt to explain this modulator role of alpha amplitude in SSDs under the spectrum of GABAergic inhibition and disinhibition that it is well known that modulate cortical synchrony in low brain frequencies (Xiao et al., 2012 ; Shaw et al., 2019). GABA neurotransmission is altered in schizophrenia playing a key role (Schmidt and Mirnics,2015). Overall, this finding can be seen as continuous and intense alertness of attentional systems in SSDs subjects (Klimesch et al., 1999). Our analysis focused on the eyes-closed task, a condition that produced more uniform and consistent findings in psychiatric disorders (Newson and Thiagarajan, 2019) than eyes-open resting-state.

We found group differences in inter-hemispheric links between the following sensors pairs :O1-P4 P3-O2 P3-T6 C3-T6 F3-O2 F3-C4 for iPLV and C3-T6 C3-T4 for corrEnv. Group-averaged iPLV values were higher for SSDs while group-averaged corrEnv were higher for healthy controls. Our findings are in conjunction with a previous study using EEG resting-state in schizophrenia (Olejarczyk and Jernajczyk2017).

This study is the first one that explored simultaneously both intra-frequency and cross-frequency interactions in both amplitude and phase domain in SSDs under DoCM model. Under this framework, we can decipher the multiplexity of complex electrophysiological aberrant connectivity observed in SSDs by integrating the available intrinsic coupling modes.

Our DoCM model untangled the multiplexity of human brain dynamics recorded with EEG by integrated both within and between frequencies coupling modes under the same framework (Buzsaki and Watson, 2012). DoCM model hypothesizes that the fluctuation of DoCM can capture the complexity of functional brain connectivity during both spontaneous and cognitive tasks. The transitive nature of DoCM across experimental time can be quantified with FI which is a direct mearure of the brain's multiplexity. FI can be seen as a reflex index that describes the readiness of the brain to respond to new stimuli.

It would be interesting to follow the same methodology during cognitive tasks and also on the source level to get the advantage of animal models, pharmaco-based studies and fMRI studies that revealed the mechanistic explanation of aberrant networks in schizophrenia (Hunt et al., 2017).

The whole study is unique, innovative, and pioneering in terms of the analytic pathway and scientific results. However, there are two basic limitations. The first refers to the interpretation of the results on the EEG surface level instead of virtual cortical sources. It would be interesting to follow the same methodological approach in an EEG study recorded healthy controls and SSDs using a large number of EEG net sensors that support the source reconstruction approach. The second drawback is the limitation of the free EEG database that involves only recordings without any access to neuropsychological assessment battery. This missing part prevented us to correlate the novel chronnectomic and semantic features with trivial neuropsychological estimates.

5. Conclusions

In the present study, we adopted a holistic approach of exploring how brain activity and connectivity mediated by intra and cross-frequency interactions differentiate in SSDs subjects compared to HC. We untangled a reconfiguration of amplitude driven DoCM in SSDs subjects mediated by alpha activity. Our findings detected significant and novel findings that will help clinicians to detect SSDs with a low cost EEG device. Concerning results to alpha frequency, alpha signal power can be used as an objective evaluator of the positive outcome of a proper neurofeedback training. Further analysis is needed to link our DoCM findings with the severity of symptoms in a cohort that will include a broader age distribution and female subjects.

Acknowledgments

I would like to thank Professor David Linden for his careful proof-reading, his thoughtful comments based on his expertise that finally improved and shaped the final paper.

I would like also to thank Professors Kaplan AI, Gorbachevskaia N L & Kozlova I. for making this dataset available to the public for further research.

SID was supported by MRC grant MR/K004360/1 (Behavioral and Neurophysiological Effects of Schizophrenia Risk Genes: A Multi-locus, Pathway Based Approach). SID is also supported by a MARIE-CURIE COFUND EU-UK Research Fellowship. We would like to acknowledge RCUK of Cardiff University and Wellcome Trust for covering the publication fee.

Conflict of Interest

The authors declare that the research was conducted in the absence of any commercial or financial relationships that could be construed as a potential conflict of interest.

Tables

Table 1. Evaluation of Classification performance based the semantic features pool of PD and FI and on a multi - kernel SVM approach.

	Accuracy	**Sensitivity**	**Specificity**
PD+FI for iPLV	74.53 $\pm$ 2.11	72.21 $\pm$ 2.31	71.85 $\pm$ 1.89
PD+FI for corrEnv	100.00 $\pm$ 0.00	100.00 $\pm$ 0.00	100.00 $\pm$ 0.00

Legends

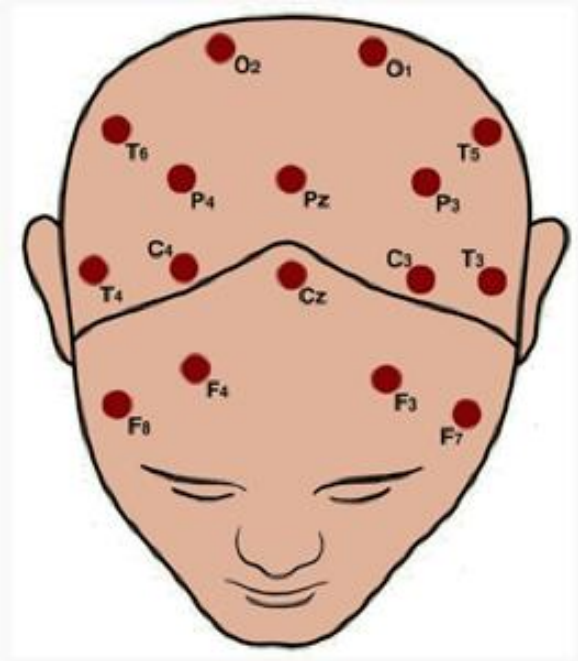

Figure 1. Topology of EEG recording sensors.

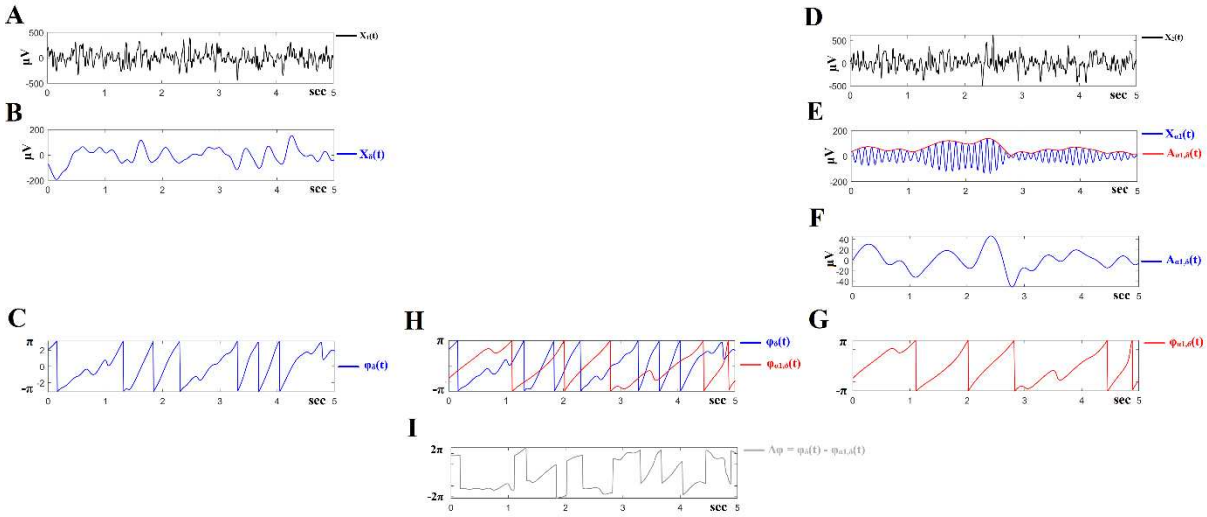

Figure 2. Outline of the PAC algorithm.

1.Preprocessing steps for F3 EEG sensor activity:

A. The time course of the first 5 secs from the F3 and F4 EEG sensor activity

B. The time course of δ activity from the F3 sensor

C. The phase time course of δ activity from F3 sensor

2.Preprocessing steps for F4 EEG sensor activity:

D. The time course of the first 5 secs from the F4 EEG sensor activity

E. The time source of α_1 activity from the F4 sensor and the δ activity extracted from α_1 activity from the same sensor. δ activity was extracted from α_1 activity using the bandpass filtering transfer functions employed to extract δ activity from the F3 sensor

F. The δ activity within α_1 activity from the F4 sensor

G.The phase temporal course of δ activity bandpass filtered from α_1 activity extracted via Hilbert transform

3.Targeted Phase Time Series for The Estimation of PAC

H. Common plot of the phase time course of δ activity from F3 sensor (C) and the phase temporal course of δ activity bandpass filtered from α_1 activity extracted via Hilbert transform (G)

I. The phase difference of the two targeted phase time series from PAC strength will be quantified via iPLV estimator

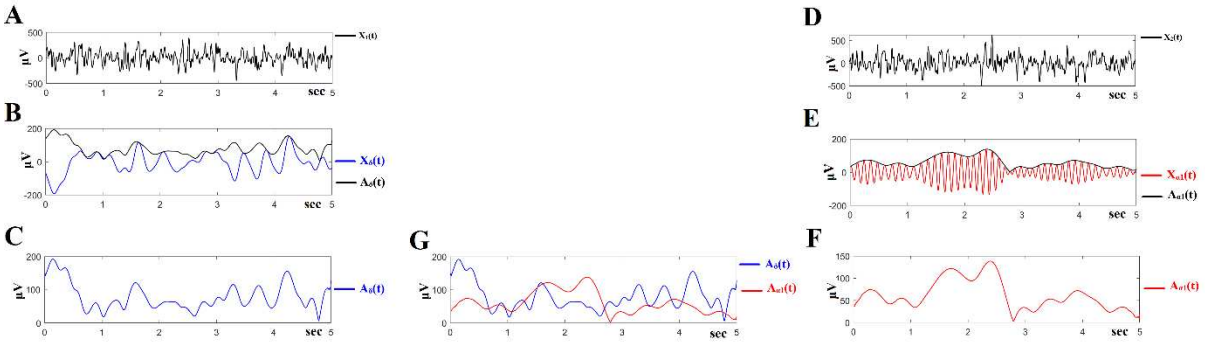

Figure 3. Outline of AAC algorithm.

1.Preprocessing steps for F3 EEG sensor activity:

A. The time course of the first 5 secs from the F3 and F4 EEG sensor activity

B. The δ activity from the F3 sensor and its related envelope extracted via Hilbert transform

C. The time course of the envelope related to δ activity of F3

2.Preprocessing steps for F4 EEG sensor activity:

D. The time course of the first 5 secs from the F4 EEG sensor activity

E. The α_1 activity from the F4 sensor and its related envelope extracted via Hilbert transform.

F. The time course of the envelope related to α_1 activity of F4 sensor

3.Targeted Phase Time Series for The Estimation of AAC

G. Common plot of both envelopes time courses of δ activity from F3 sensor (C) and of α_1 activity extracted via Hilbert transform (F). AAC is estimated between those time courses via a correlation envelope analysis (corrEnv).

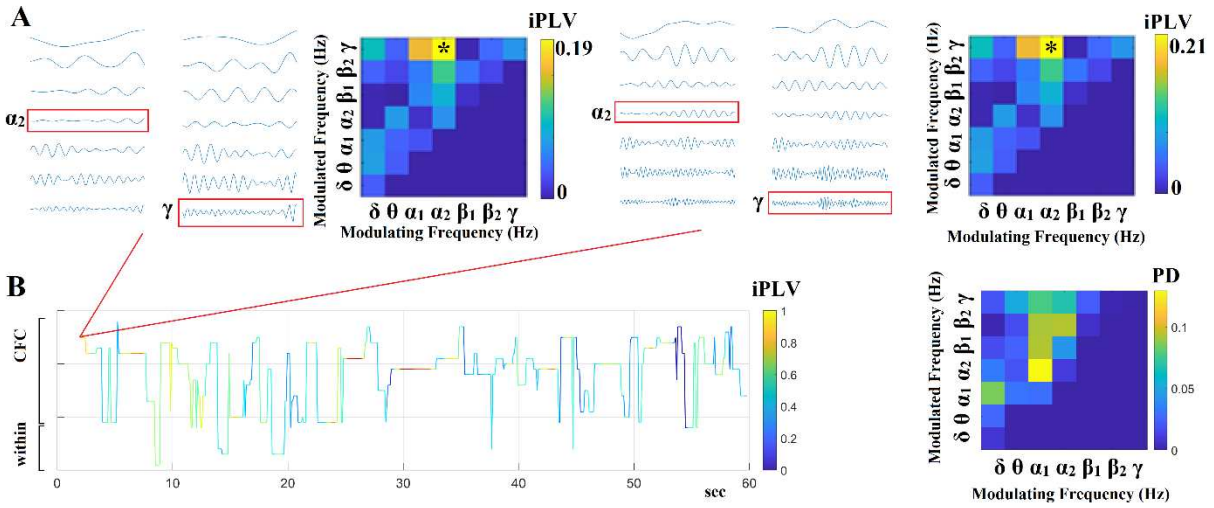

Figure 4. Determining Dominant Intrinsic Coupling Modes (DoCM) based on iPLV.
(A) A detailed schematic illustration of the adapted DoCM model showing the detection of dominant coupling mode between two EEG sensors (F3 and F7) for the first two consecutive temporal segment (ts_1, ts_2). For demonstration purpose, we adapted imaginary Phase Locking (iPLV) which was employed for the estimation of both within frequencies (e.g., δ to δ) and between frequencies (cross-frequency) interactions (e.g., δ to θ). Surrogate analysis will reveal the DoCM for both temporal segments. During ts_1 the DoCM reflected significant phase locking between α_2 and γ oscillations (indicated by red rectangles) while during in ts_2 the dominant interaction was remain stable.
(B) Burst of DoCM between the F3 and F7 sensors. This streaming of the basic elements of neural communication is encapsulated in the DoCM time series to form a neural "word.", which can be interpreted as a spatio-temporal message in the macroscale level (Buzsaki & Watson, 2012). The plot illustrates the fluctuation of DoCM across experimental time for F3-F7 sensor pair. Y-axis refers to one of the 28 potential coupling modes while the colour refers to the iPLV related strength. The first two temporal segment showed in A. revealed α_2 - γ as DoCM. This observation is shown in the first samples of the time-source showed in B. FI is estimated based on such a semantic time series by counting how many times the DoCM changed between consecutive temporal segments divided by the total number of temporal segments -1. FI ranged within [0,1] where higher values are interpreted as higher flexibility.
The comodulogram on the right demonstrates the probability distribution (PD) of the DoCM across temporal segments for the EEG sensor pair F7-F3. α_1-α_2 is the CFC with the highest representation across experimental time for this EEG pair of sensors
The outcome of this approach is the construction of 2 DFCG represented as 3D tensors of size [1275 x 16 x 16] .

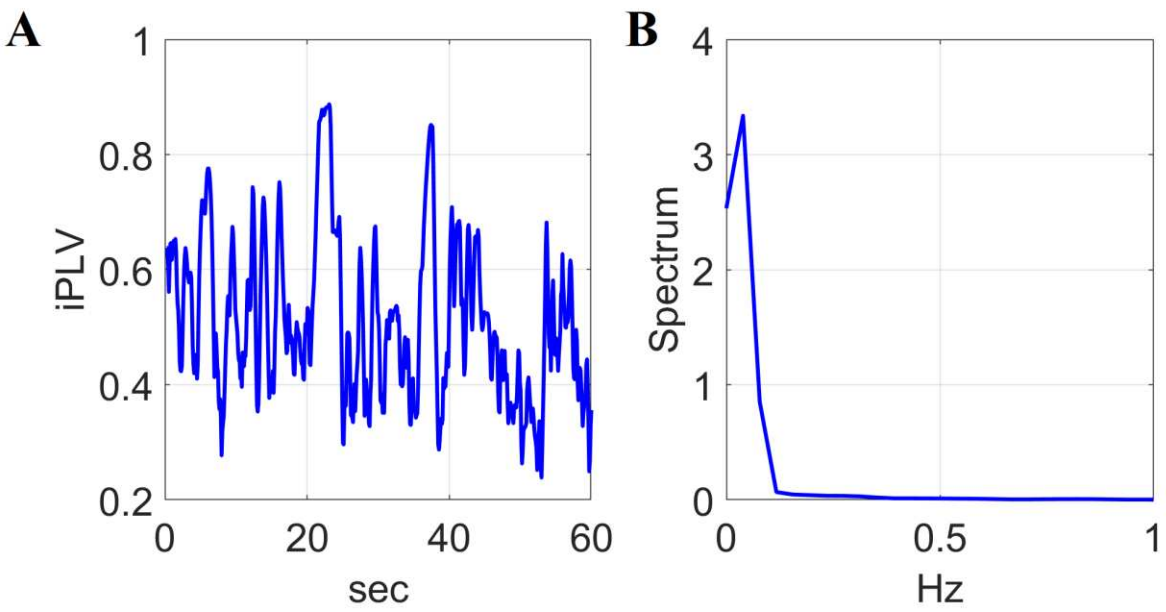

Figure 5. Inter-hemispheric fluctuations and the related dominant frequency
A illustrates an example of a time series presenting the temporal functional strength between F7-F8 EEG sensors from the first healthy control subject. The spectrogram of this dynamic functional strength was extracted and the related dominant frequency is assigned to this inter-hemispheric pair as descriptive statistic of the fluctuation of connectivity across experimental time (B).

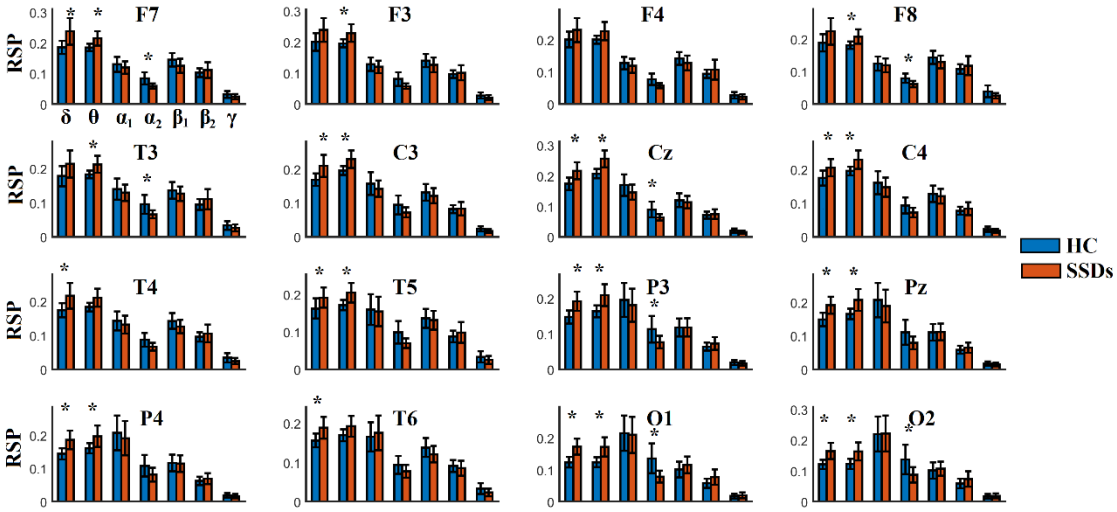

Figure 6. Group-Averaged Relative Signal Power (RSP) across EEG sensor space and frequency bands in HC and SSDS patients.
Our analysis revealed significant higher δ RSP for SSDs compared to HC in O1 and O2 EEG sensors.
(* Wilcoxon Rank Sum test ($p < 0.01$, Bonferroni corrected, $p' < p/(16*7)$ where 16 refers to EEG sensors and 7 to the number of the studying frequency bands).

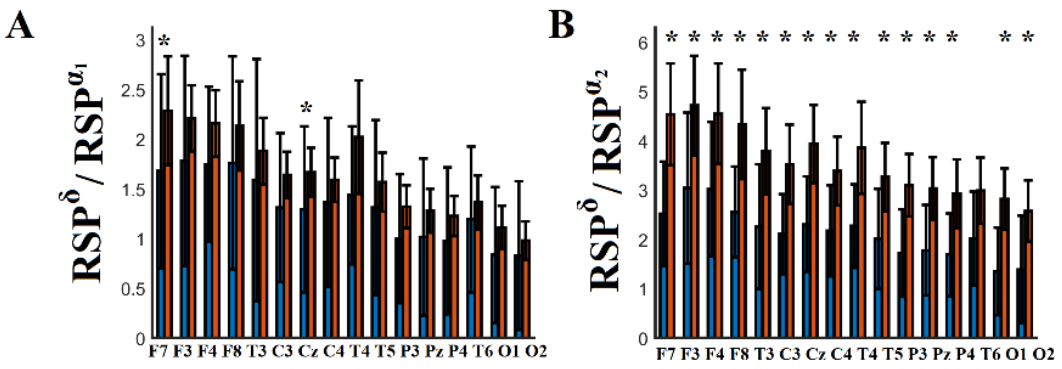

Figure 7. Group-averaged Ratio of Relative Signal Power (RSP) of δ versus RSP of α_1 and α_2 across EEG sensor space in HC and SSDs patients.
Our analysis revealed significant higher ratio of RSP of **δ with α_1** for SSDS compared to HC in F7 and Cz EEG sensors.
Significant higher ratio RSP of **δ with α_2** for SSDS compared to HC were revealed in all the EEG sensors with the exception of T6 EEG sensors.
(* Wilcoxon Rank Sum test ($p < 0.01$, Bonferroni corrected, $p' < p/(16*2)$ where 16 refers to EEG sensors and 2 to the number of the ratios).

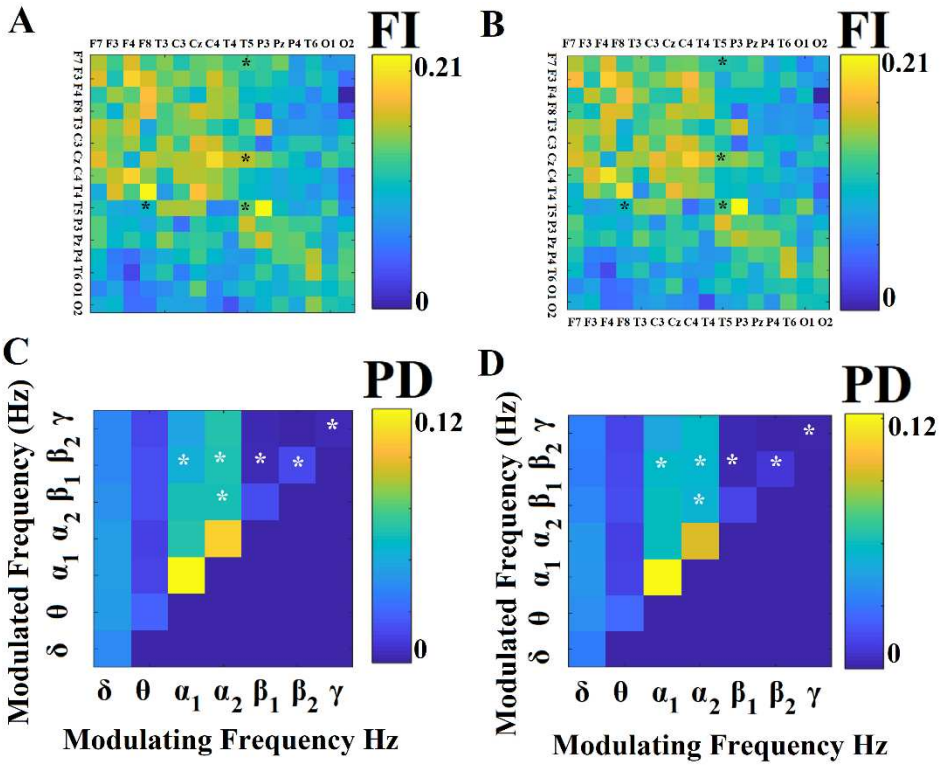

Figure 8. Group-Averaged Flexibility Index (FI) and Comodulograms that tabulate the PD of spatio-temporally DoCM based on iPLV estimator.
(A-B) Group-averaged FI for healthy control (HC) group (A) and group with schizophrenia-spectrum disorders (SSDs) (B).
(C-D) Group-averaged comodulograms for HC and SSDs group, correspondingly
Every FI and PD has been selected via the feature selection algorithm is denoted with '*'.

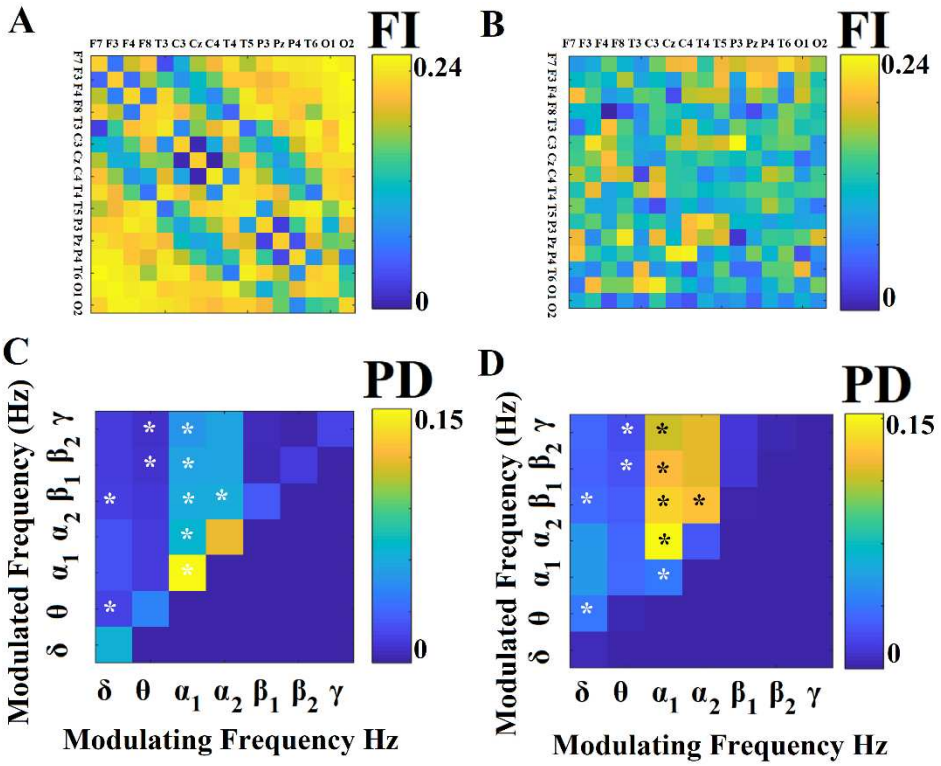

Figure 9. Group-Averaged Flexibility Index (FI) and Comodulograms that tabulate the PD of spatio-temporally DoCM based on corrEnv estimator.
(A-B) Group-averaged FI for healthy control (HC) group (A) and group with schizophrenia-spectrum disorders (SSDs) (B).
(C-D) Group-averaged comodulograms for HC and SSDs group, correspondingly
Every FI and PD has been selected via the feature selection algorithm is denoted with '*'.

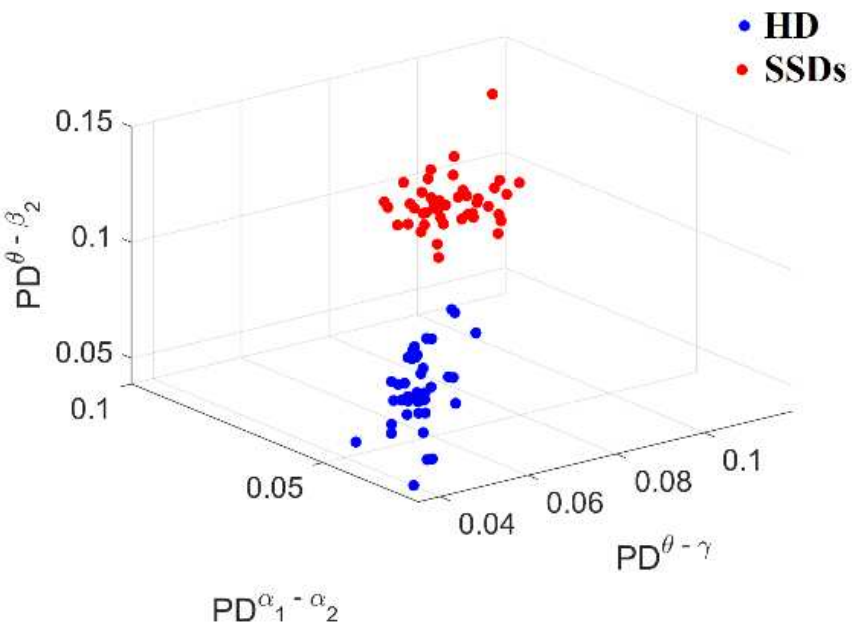

Figure 10. Discriminative power of PD for θ-γ, α_1-α_2 θ-β_2 cross-frequency pairs. Every dot corresponds to a single subject.

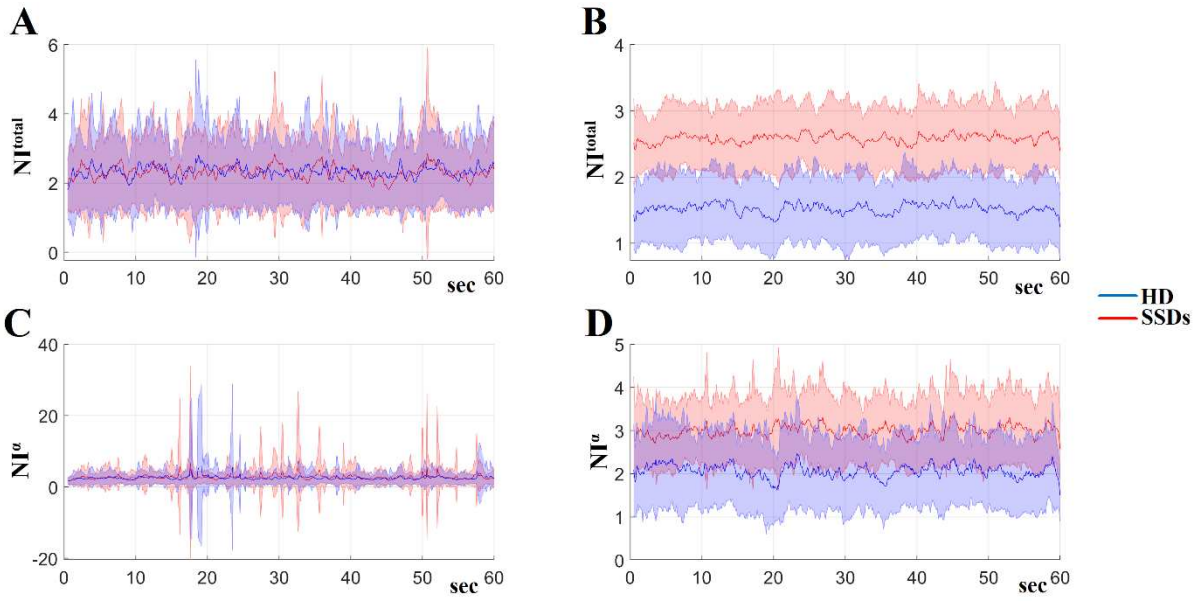

Figure 11. Group –averaged Nonlinearity Index across experimental time .

A) NI^{Total} for iPLV,

B) NI^{Total} for corrEnv,

C) NI^{α} for iPLV

D) NI^{α} for corrEnv

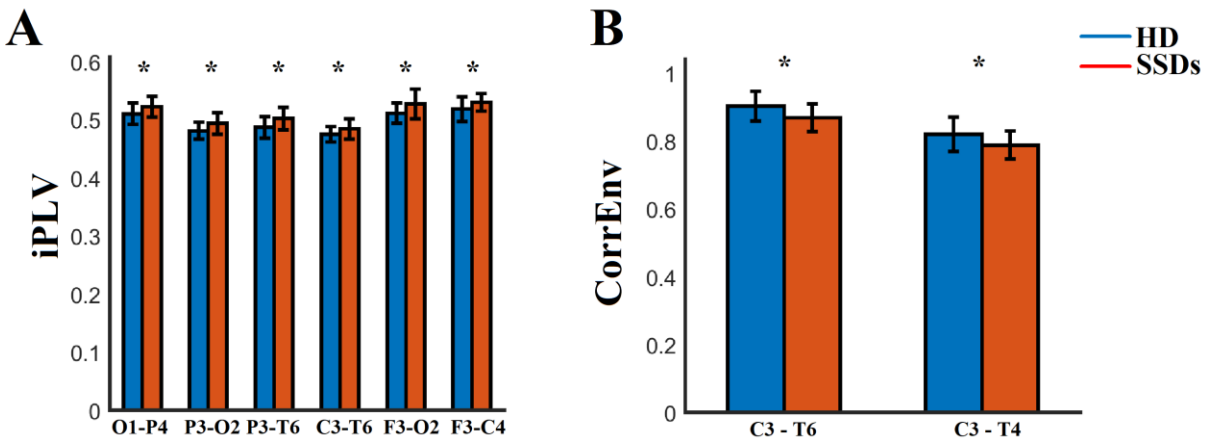

Figure 12. We found group-averaged differences between the mean values of the following inter-hemispheric links :O1-P4 P3-O2 P3-T6 C3-T6 F3-O2 F3-C4 (Figure 12.A), for iPLV and C3-T6 C3-T4 for corrEnv (B).

References

Alfimova MV, Uvarova LG. Changes in EEG spectral power on perception of neutral and emotional words in patients with schizophrenia, their relatives, and healthy subjects from the general population. Neurosci Behav Physiol. 2008;38(5):533-40.

Allen EA, Lin J, Kiehl KA, Gelernter J, Pearlson GD, Perrone-Bizzozero NI, Calhoun VD (2011). Components of cross-frequency modulation in health and disease. Front Syst Neurosci. 5:59

Andreou C, Leicht G, Nolte G, Polomac N, Moritz S, Karow A, et al. Resting-state theta-band connectivity and verbal memory in schizophrenia and in the high-risk state. Schizophr Res 2015;161(2–3):299–307.

Antonakakis, M., Dimitriadis, S. I., Zervakis, M., Micheloyannis, S., Rezaie, R., Babajani-Feremi, A.,Papanicolaou, A. C. Altered crossfrequency coupling in resting-state MEG after mild traumatic brain injury. Int J Psychophysiol 2016;102:1–11.

Antonakakis, M., Dimitriadis, S. I., Zervakis, M., Papanicolaou, A. C., & Zouridakis, G. . Reconfiguration of dominant coupling modes in mild traumatic brain injury mediated by δ-band activity: A resting state MEG study. Neuroscience 2017;25(356):275–286.

Antonakakis, M., Dimitriadis, S. I., Zervakis, M., Papanicolaou, A. C., & Zouridakis, G. Altered rich-club and frequency-dependent subnetwork organization in mild traumatic brain injury: A MEG resting- state study. Front Hum Neurosci 2017;11; 416. eCollection. https://doi.org/10.3389/fnhum.2017.00416

Basar, E. & Guntekin, B. Review of delta, theta, alpha, beta, and gamma response oscillations in neuropsychiatric disorders. Suppl. Clin. Neurophysiol. 2013;62:303–341.

Basar, E., Basar-Eroglu, C., Guntekin, B. & Yener, G. G. Brain's alpha, beta, gamma, delta, and theta oscillations in neuropsychiatric diseases: proposal for biomarker strategies. Suppl. Clin. Neurophysiol. 2013;62:19–54.

Borisov, S. V., Kaplan, A. I., Gorbachevskaia, N. L. & Kozlova, I. A. Segmental structure of the EEG alpha activity in adolescents with disorders of schizophrenic spectrum. Zh. Vyssh. Nerv. Deiat. Im. I. P. Pavlov. 2005;55:329–335.

Breakspear M(2002) Nonlinear phase desynchronization in human electroencephalographic data. Hum Brain Mapp 15:175–198.

Buzsáki, G., & Watson, B. O. Brain rhythms and neural syntax: Implications for efficient coding of cognitive content and neuropsychiatric disease. Dialogues in Clin Neurosci 2012;14(4):345–367.

Canolty RT, Knight RT. The functional role of cross-frequency coupling. Trends Cogn. Sci. 2010; 14(11): 506–515.

Chen CC, Henson RN, Stephan KE, Kilner JM, Friston KJ (2009) Forward and backward connections in the brain: a DCM study of functional asymmetries. Neuroimage 45:453–462.

Chen, C. C., Kilner, J. M., Friston, K. J., Kiebel, S. J., Jolly, R. K., and Ward, N. S. (2010). Nonlinear coupling in the human motor system. *J. Neurosci*. 30, 8393–8399.

Chen Y-H, Stone-Howell B, Edgar JC, Huang M, Wootton C, Hunter MA et al. Frontal slow-wave activity as a predictor of negative symptoms, cognition and functional capacity in schizophrenia. Br J Psychiatry 2016;208(02), 160–167.

Chung, Fan (1997). Spectral Graph Theory. American Mathematical Society.

Corcoran AM, Alday PM, Schlesewsky M. Toward a reliable, automated method of individual alpha frequency (IAF) quantification. Psychophysiology 2018;55:Article e13064

Courvoisie H, Labellarte MJ, Riddle MA. Psychosis in children: diagnosis and treatment. Dialog Clin Neurosci 2001; 3: 79–92

Corbetta, M. & Shulman, G. L. Control of goal-directed and stimulus-driven attention in the brain. Nat. Rev. Neurosci. 2002;3:201–215.

Darvas F, Miller KJ, Rao RPN, Ojemann JG.Nonlinear Phase–Phase Cross-Frequency Coupling Mediates Communication between Distant Sites in Human Neocortex. J Neurosci. 2009 Jan 14; 29(2): 426–435.

Delorme, A., & Makeig, S.. EEGLAB: An open source toolbox for analysis of single-trial EEG dynamics including independent component analysis. J Neurosci Meth. 2004;134:9–21.

DeRosse P, Karlsgodt KH. Examining the Psychosis Continuum. Current behavioral neuroscience reports. 2015;2:80-89

Di Lorenzo G, Daverio A, Ferrentino F, Santarnecchi E, Ciabattini F, Monaco L, et al. Altered resting-state EEG source functional connectivity in schizophrenia: the effect of illness duration. Front Hum Neurosci. 2015;9:234.

Dimitriadis SI, LaskarisN A, & Tzelepi A. On the quantizationof time-varying phase synchrony patterns into distinct Functional Connectivity Microstates (FCμstates) in a multi-trial visual ERP paradigm. Brain Topogr.2013;26:397–409.

Dimitriadis SI, Laskaris NA, Simos PG, Micheloyannis S, FletcherJM, Rezaie R, & Papanicolaou, AC. Altered temporal correlations in resting-state connectivity fluctuations in children with reading difficulties detected via MEG. Neuroimage 2013;83: 307–317.

Dimitriadis S I, Laskaris NA, Bitzidou MP, Tarnanas I, & TsolakiM. (2015a). A novel biomarker of amnestic MCI based on dynamic cross-frequency coupling patterns during cognitive brain responses. Front Neurosci 2015;9:350.

Dimitriadis SI, Laskaris NA, & Micheloyannis S. . Transition dynamics of EEG-based network microstates unmask developmental and task differences during mental arithmetic and resting wakefulness. Cogn Neurodynamics 2015;9:371–387.

Dimitriadis SI, Laskaris N A, Simos G, Fletcher J, & Papanicolaou A CGreater repertoire and temporal variability of Cross-Frequency Coupling (CFC) modes in resting-state neuromagnetic recordings among children with reading difficulties. Front Hum Neurosci 2016;10:63.

Dimitriadis S I, SunY, Laskaris N, Thakor N, & Bezerianos A.Revealing cross-frequency causal interactions during a mental arithmetic task through symbolic transfer entropy: A novel vectorquantization approach. IEEE Trans Neural Syst Rehabil Eng 2016;24:1017–1028.

Dimitriadis SI, Tarnanas I, Wiederholdg M, Wiederholdh B, Tsolaki M, Fleische E. Mnemonic strategy training of the elderly at risk for dementia enhances integration of information processing via cross-frequency coupling. Alzheimers Dement (N Y) 2016;2:241–249.

Dimitriadis S I, Salis C, Tarnanas I, Linden D. Topological filtering of dynamic functional brain networks unfolds informative chronnectomics: a novel data-driven thresholding scheme based on orthogonal minimal spanning trees (OMSTs). Front. Neuroinform. 2017;11:28.

Dimitriadis S I, and Salis CI Mining time-resolved functional brain graphs to an EEG-based chronnectomic brain aged index (CBAI). Front. Hum. Neurosci. 2017;11:423.

Dimitriadis SI, Antonakakis M, Simos P, Fletcher JM, and Papanicolaou A. Data-driven topological filtering based on orthogonal minimal spanning trees: application to multi-group MEG resting-state connectivity. Brain Connect. 2017;7:661–670.

Dimitriadis S I, López ME, Bruña R, Cuesta P, Marcos A, Maestú F, et al. How to build a functional connectomic biomarker for mild cognitive impairment from source reconstructed MEG resting-state activity: the combination of ROI representation and connectivity estimator matters. Front. Neurosci. 2018;12:306.

Dimitriadis SI, Routley B, Linden D E, & Singh K D.Reliability of static and dynamic network metrics in the resting-state: A MEG-beamformed connectivity analysis.Front. Neurosci. 2018; 12: 506.

Dimitriadis SI . Complexity of brain activity and connectivity in functional neuroimaging.J Neurosci Res. 2018;96(11):1741-1757.

Dimitriadis SI, P. Simos, J. Fletcher, A. Papanicolaou.Aberrant resting-state functional brain networks in dyslexia: symbolic mutual information analysis of neuromagnetic signals. Int. J. Psychophysiol. 2018;126;20-29

Dimitriadis, S.I.; Simos, P.G.; Fletcher, J.M.; Papanicolaou, A.C. Typical and Aberrant Functional Brain Flexibility: Lifespan Development and Aberrant Organization in Traumatic Brain Injury and Dyslexia. *Brain Sci.* **2019**;*9*:380.

Dvey-Aharon Z, N. Fogelson, A. Peled, N.IntratorConnectivity maps based analysis of EEG for the advanced diagnosis of schizophrenia attributes. PLoS One, 2017;12: Article e0185852,

Engel AK, Gerloff C, Hilgetag CC& Nolte G. Intrinsic coupling modes: multiscale interactions in ongoing brain activity. Neuron 2013;80:867–886.

Englehardt, W., Carl, G., Dierks, T. & Maurer, K. Electroencephalographic mapping during isoflurane anesthesia for treatment of mental depression. J. Clin. Monit. 1991;7:23–29.

Florin E, Baillet S. The brain's resting-state activity is shaped by synchronized cross-frequency coupling of neural oscillations. Neuroimage 2015 1;111:26-35.

Fox M D, Corbetta M, Snyder A Z, Vincent J L. & Raichle M E. Spontaneous neuronal activity distinguishes human dorsal and ventral attention systems. Proc Natl Acad Sci USA 2006;103(26):10046-10051

Fuller P, Sherman D, Pedersen NP, Saper CB, Lu J. Reassessment of the structural basis of the ascending arousal system. The Journal of comparative neurology. 2011;519:933–956.

Friston KJ, Frith CD. Schizophrenia: a disconnection syndrome? Clin Neurosci 1995; 3: 88–97.

Friston K, Brown HR, Siemerkus J, Stephan KE. The dysconnection hypothesis (2016). Schizophr Res. 2016;176:83–94.

Gianotti L. R. R., Kunig G., Faber P. L., Lehmann D., Pascual-Marqui R. D., Kochi K., et al. (2008). Rivastigmine effects on EEG spectra and three-dimensional LORETA functional imaging in Alzheimer's disease. Psychopharmacology 2018;198:323–332

Gonzalez-Burgos, G., and Lewis, D. A.NMDA receptor hypofunction, parvalbumin-positive neurons and cortical gamma oscillations in schizophrenia. *Schizophr. Bull.* 2012;38: 950–957.

Gotts SJ, Jo HJ, Wallace GL, Saad ZS, Cox RW, Martin A. Two distinct forms of functional lateralization in the human brain. Proc Natl Acad Sci U S A. 2013;110(36):E3435–44.

Hashemi, M., Hutt, A. & Sleigh, J. How the cortico-thalamic feedback affects the EEG power spectrum over frontal and occipital regions during propofolinduced sedation. J. Comput. Neurosci. 2015;39:155–179.

Herrera, C. G. et al. Hypothalamic feedforward inhibition of thalamocortical network controls arousal and consciousness. Nat. Neurosci. 2016;19:290–298

Hinkley LB, Vinogradov S, Guggisberg AG, Fisher M, Findlay AM, Nagarajan SS. Clinical symptoms and alpha band resting-state functional connectivity imaging in patients with schizophrenia: implications for novel approaches to treatment. Biol Psychiatry. 2011;70(12):1134–42.

Hoffman, W. E., Charbel, F. T., Edelman, G., Albrecht, R. F. & Ausman, J. I. Nitrous oxide added to isoflurane increases brain artery blood flow and low frequency brain electrical activity. J. Neurosurg. Anesthesiol. 1995;7:82–88.

Howells FM, Temmingh HS, Hsieh JH, van Dijen AV, Baldwin DS, Stein DJ. Electroencephalographic delta/alpha frequency activity differentiates psychotic disorders: a study of schizophrenia, bipolar disorder and methamphetamine-induced psychotic disorder. Transl Psychiatry. 2018;8(1):75.

Hughes, S. W., and Crunelli, V. Thalamic mechanisms of EEG alpha rhythms and their pathological implications. *Neuroscientist* 2005;11:357–372.

Hunt MJ, N.J. Kopell, R.D. Traub, M.A. Whittington.Aberrant network activity in schizophrenia. Trends Neurosci 2017;40:371-382

Hyafil A, Giraud AL, Fontolan L, Gutkin B. Neural Cross-Frequency Coupling: Connecting Architectures, Mechanisms, and Functions.Trends Neurosci. 2015;38(11):725-740.

Ingwar DH, Franzen G. Abnormalities of cerebral blood flow distribution in patients with chronic schizophrenia. Acta Psychiat. Scand. 1974; 50: 425–462.

Javitt, D. C. Glutamatergic theories of schizophrenia. *Isr. J. Psychiatry Relat. Sci.* 2010;47:4–16.

John, J. P., Khanna, S., Pradhan, N. & Mukundan, C. R. EEG alpha coherence and psychopathological dimensions of schizophrenia. Indian J. Psychiatry 2002;44:97–107 .

Jensen O, Colgin LL (2007) Cross-frequency coupling between neuronal oscillations. Trends Cogn Sci 11:267–269.

Kam JW, Bolbecker AR, O'Donnell BF, Hetrick WP, Brenner CA. Resting state EEG power and coherence abnormalities in bipolar disorder and schizophrenia. J Psychiatr Res. 2013;47(12):1893–901.

Kaplan RF, Glueck BC, Hesselbrock MN, Reed HBJr. Power and coherence analysis of the EEG in hospitalized alcoholics and nonalcoholic controls. J. Stud. Alcohol 1985;46:122–127.

Kaymax N., Drukker M., Lieb R., Wittchen H.-U., Werbeloff N., Weiser M., et al. Do subthreshold psychotic experiences predict clinical outcomes in unselected non-help-seeking population-based samples? A systematic review and meta-analysis, enriched with new results. Psychol. Med. 2012;42:2239–2253.

Klimesch, W. EEG alpha and theta oscillations reflect cognitive and memory performance: a review and analysis. Brain. Res. Brain. Res. Rev. 1999;29:169–195.

Kulaichev AP, Natalia Gorbachevskaya L. Differentiation of norm and disorders of schizophrenic spectrum by analysis of EEG correlation synchrony. J Exp Integr Med. 2013; 3(4): 267-278

Kwapil TR, Barrantes-Vidal N. Schizotypy:looking back and moving forward.Schizophr. Bull, 41;S336-S373.

Lehembre R, MarieAurélie B, Vanhaudenhuyse A, Chatelle C, Cologan V, Leclercq Y, Soddu A, Macq B, LaureysS, Noirhomme Q.Resting-state EEG study of comatose patients: a connectivity and frequency analysis to find differences between vegetative and minimally conscious statesFunct. Neurol. 2012;27:41–47.

Lehmann D, Faber PL, Pascual-Marqui RD, Milz P, Herrmann WM, Koukkou M, et al. Functionally aberrant electrophysiological cortical connectivities in first episode medication-naive schizophrenics from three psychiatry centers. Front Hum Neurosci. 2014;8:635.

Linscott R. J., van Os J. . An updated and conservative systematic review and meta-analysis of epidemiological evidence on psychotic experiences in children and adults: on the pathway

from proneness to persistence to dimensional expression across mental disorders. Psychol. Med. 43;1133–1149.

Lisman J, and Buzsaki G. A Neural Coding Scheme Formed by the Combined Function of Gamma and Theta Oscillations. Schizophr. Bull. 2008; 34: 974

Maran M, T. Grent-t-Jong, P.J. Uhlhaas. Electrophysiological insights into connectivity anomalies in schizophrenia: a systematic review. Neuropsychiatr Electrophysiol2016;2(6)

Márton CD, M Fukushima, CR Camalier, SR Schultz, BB Averbeck.
Signature patterns for Top-Down and Bottom-Up information processing via Cross-Frequency coupling in macaque auditory cortex. Eneuro 2019;6:ENEURO.0467-18.2019.

Merrin EL, Floyd TC. Negative symptoms and EEG alpha in schizophrenia: a replication. Schizophr Res. 1996; 19(2–3):151–161

Mitchell AC, Jiang Y, Peter C, Akbarian S. Transcriptional regulation of GAD1 GABA synthesis gene in the prefrontal cortex of subjects with schizophrenia. Schizophr Res . 2015;167:28-34.

Miyata J, Sasamoto A, Koelkebeck K, Hirao K, Ueda K, Kawada R, et al. Abnormal Asymmetry of White Matter Integrity in Schizophrenia Revealed by Voxelwise Diffusion Tensor Imaging. Human Brain Mapping 2012; 33:1741–1749.

Moran LV, L.E. Hong.High vs low frequency neural oscillations in schizophreniaSchizophr Bull 2011;37:659-663

Mubarik, A. & Tohid, H. Frontal lobe alterations in schizophrenia: a review. *Trends Psychiatry Psychother.* **38**, 198–206 (2016).

Newson, J. J., and Thiagarajan, T. C. (2019). EEG frequency bands in psychiatric disorders: a review of resting state studies. Front. Hum. Neurosci. 12:521.

Nunez, P. L., and Srinivasan, R. (2006). *Electric Fields of the Brain: The Neurophysics of EEG, 2nd Edn*. New York, NY: Oxford University Press

Oertel-Knoechel V, Knoechel C, Staeblein M, Linden DE. Abnormal Functional and Structural Asymmetry as Biomarker for Schizophrenia. Current Topics in Medicinal Chemistry 2012; 12(21): 2434–2451.

Olejarczyk, E, Jernajczyk, W. Graph-based analysis of brain connectivity in schizophrenia. PLoS One. 2017;12:e0188629.

Olincy, A., and Freedman, R. Nicotinic mechanisms in the treatment of psychotic disorders: a focus on the alpha7 nicotinic receptor. *Handb. Exp. Pharmacol.* 2012;213:211–232.

Ragland JD, Yoon J, Minzenberg MJ, Carter CS. Neuroimaging of cognitive disability in schizophrenia: Search for a pathophysiological mechanism. Int Rev Psychiatry 2007; 19(4): 417–427.

Ribolsi M, Daskalakis ZJ, Siracusano A, Koch G. Abnormal asymmetry of brain connectivity in schizophrenia. Front Hum Neurosci 2014; 8: 1010

Roffo, G., Melzi, S. and Cristani, M. Infinite feature selection. In: Proceedings of the IEEE International Conference on Computer Vision 2015;4202-4210

Rössler W, Ajdacic-Gross V, Müller M, Rodgers S, Haker H, Hengartner MP. Assessing sub-clinical psychosis phenotypes in the general population--a multidimensional approach. Schizophr Res. 2015;161(2-3):194–201.

Schmitt A, Hasan A, Gruber O, Falkai P. Schizophrenia as a disorder of disconnectivity. Eur Arch Psychiatry Clin Neurosci. 2011; 261 Suppl 2:S150–4.

Sekimoto, M., Kato M, Watanabe T, Kajimura N, Takahashi K.(2010) Cortical regional differences of delta waves during all-night sleep in schizophrenia, Schizophr Res. 2011 Mar;126(1-3):284-90.

Sharp FR, Hendren RL. Psychosis: atypical limbic epilepsy versus limbic hyperexcitability with onset at puberty? Epilepsy Behav 2007;10: 515–520

Shaw AD, Knight L, Freeman TCA, Williams GM, Moran RJ, Friston KJ, et al. Oscillatory, Computational, and Behavioral Evidence for Impaired GABAergic Inhibition in Schizophrenia. Schizophr Bull. 2019. pmid:31219602.

Siems M, Siegel M.Dissociated neuronal phase- and amplitude-coupling patterns in the human brain. NeuroImage 2020;209(1);116538

Schmidt M. J., Mirnics K. Neurodevelopment, GABA system dysfunction, and schizophrenia. Neuropsychopharmacology 2015;40:190–206. 10.1038/npp.2014.95

Tallon-Baudry C, Bertrand O (1999) Oscillatory gamma activity in humans and its role in object representation. Trends Cogn Sci 3:151–162.

Tauscher J, Fischer P, Neumeister A, Rappelsberger P, Kasper S. Low frontal electroencephalographic coherence in neuroleptic-free schizophrenic patients. Biol Psychiatry. 1998;44(6):438–47.

Ulrich, D. Subthreshold delta-frequency resonance in thalamic reticular neurons. Eur. J. Neurosci. 40, 2600–2607 (2014).

Unterrassner L, Wyss TA, Wotruba D, Ajdacic-Gross V, Haker H, Rössler W. Psychotic-Like Experiences at the Healthy End of the Psychosis Continuum. Front Psychol. 2017;8:775.

van Driel J, Cox R, Cohen MX. Phase-clustering bias in phase amplitude cross-frequency coupling and its removal. J Neurosci Meth 2015;254:60 –72.

Van Os J., Hanssen M., Bijl R. V., Ravelli A. Strauss (1969) revisited: a psychosis continuum in the general population? Schizophr. Res. 2000;45;11–20.

van Os J., Linscott R. J., Myin-Germeys I., Delespaul P., Krabbendam L. A systematic review and meta-analysis of the psychosis continuum: evidence for a psychosis proneness-persistence-impairment model of psychotic disorder. Psychol. Med. 2009;39:179–195.

van Os J., Linscott R. J. (2012). Introduction: the extended psychosis phenotype—relationship with schizophrenia and with ultrahigh risk status for psychosis. Schizophr. Bull. 2012;38:227–230.

Hill K, Varese F, Jackson M, Linden DE.The relationship between metacognitive beliefs, auditory hallucinations, and hallucination-related distress in clinical and non-clinical voice-hearers. Br J Clin Psychol. 2012;51:434–447

Vanderwolf CH, Pappas BA. Reserpine abolishes movement-correlated atropine-resistant neocortical low voltage fast activity. Brain research. 1980;202:79–94.

Varela F, Lachaux JP, Rodriguez E, Martinerie J (2001) The brainweb: phase synchronization and large-scale integration. Nat Rev Neurosci 2:229–239.

Volavka, J., Matousek, M. & Roubicek, J. Mental arithmetic and eye opening. An EEG frequency analysis and GSR study. Electroencephalogr. Clin. Neurophysiol. 1967;22:174–176 .

von Stein A, Sarnthein J. Different frequencies for different scales of cortical integration: from local gamma to long range alpha/theta synchronization. Int. J. Psychophysiol. 2000; 38: 301–313.

Winterer G, Egan MF, Radler T, Hyde T, Coppola R, Weinberger DR. An association between reduced interhemispheric EEG coherence in the temporal lobe and genetic risk for schizophrenia. Schizophr Res. 2001;49(1–2):129–43.

Xiao Y., Huang X. Y., Van Wert S., Barreto E., Wu J. Y., Gluckman B. J., et al. The role of inhibition in oscillatory wave dynamics in the cortex. Eur. J. Neurosci. 2012;36:2201–2212. 10.1111/j.1460-9568.2012.08132.x

Yung A. R., Yuen H. P., Phillips L. J., Francey S., McGorry P. D. Mapping the onset of psychosis: the comprehensive assessment of at risk mental states (CAARMS). Schizophr. Res. 2003;60:30–31.

Zammit S., Kounali D., Cannon M., David A., Gunnell D., Heron J., et al. Psychotic experiences and psychotic disorders at age 18 in relation to psychotic experiences at age 12 in a longitudinal population-based cohort study. Am. J. Psychiatry 2013;170:742–750.

Zhang Y, T. Yoshida, D.B. Katz, J.E. Lisman. NMDAR antagonist action in thalamus imposes delta oscillations on the hippocampus J. Neurophysiol., 2012;107:3181-3189

Zhang T, Koutsouleris N, Meisenzahl E, Davatzikos C. Heterogeneity of structural brain changes in subtypes of schizophrenia revealed using magnetic resonance imaging pattern analysis. Schizophr Bull 2014;41: 74–84.